Lithos 206–207 (2014) 435–453

Contents lists available at ScienceDirect

Lithos

journal homepage: www.elsevier.com/locate/lithos

Fluid systems above basement shear zones during inversion of pre-orogenic sedimentary basins (External Crystalline Massifs, Western Alps)

Alexandre Boutoux [a,b,*], Anne Verlaguet [a,b], Nicolas Bellahsen [a,b], Olivier Lacombe [a,b], Benoit Villemant [a,b], Benoit Caron [a,b], Erwan Martin [a,b], Nelly Assayag [c], Pierre Cartigny [c]

[a] Sorbonne Universités, UPMC Univ. Paris 06, UMR 7193, ISTeP, F-75005 Paris, France
[b] CNRS, UMR 7193, ISTeP, F-75005 Paris, France
[c] Equipe de Géochimie des Isotopes Stables de l'Institut de Physique du Globe de Paris, Sorbonne Paris Cité, Université Paris Diderot, UMR 7154 CNRS, F-75005 Paris, France

ARTICLE INFO

Article history:
Received 9 February 2014
Accepted 5 July 2014
Available online 21 July 2014

Keywords:
Western Alps
Shear zone
Trace elements
Stable isotopes
Fluid circulations
Closed system

ABSTRACT

In the inner part of the External Alps, inherited Liassic basins were buried and inverted during the Oligo-Miocene collisional phase of the Alpine orogeny. In northern Oisans, during crustal shortening, the basement was locally sheared while the cover was disharmonically folded above the main basement shear zones that did not propagate into the cover. In this contribution, we analyze the witnesses of paleo-fluid circulations associated with these crustal deformations, focusing particularly on Bourg d'Oisans and Mizoën basins (external Western Alps). On the basis of structural and microstructural observations coupled to geochemical analyses (cathodoluminescence, O and C stable isotopes, trace elements) of vein versus host-rock minerals, we show that in the cover, fluids mainly circulated over short distances (closed-system). However, trace element data also show that percolation of small amounts of basement-derived fluids occurred over several tens of meters in cover rocks right above basement shear zones. Indeed, the three successive vein sets recognized in the field display enrichments in basement-derived Ni, Co, and Cr, which indicate that fluid transfer from the basement was efficient since the beginning of basin inversion, therefore confirming the synchronous deformation of cover and basement. Fluid temperatures and pressures are estimated (microthermometry coupled to $\delta^{18}O$ of vein minerals) to about 250–400 °C and 2–5 kbar for veins that most likely formed at or close to metamorphic peak conditions. These results coupled to literature data are finally integrated into a model of fluid circulation evolution through progressive deformation of the whole external Western Alps.

1. Introduction

In convergent settings (subduction or collision), large amounts of fluids are released in rocks by successive metamorphic dehydration reactions occurring during burial (e.g., Walther and Orville, 1982). The occurrence of fluids in rocks, in particular water, has crucial effects not only on the scale of mass transfer processes and fluid–rock interactions (e.g., John et al., 2012; Penniston-Dorland et al., 2010), but also on the deformation mechanisms and rock rheology (e.g., Bos and Spiers, 2000, 2002; Gueydan et al., 2004; and references therein). Moreover, there is a strong link between mass transfer and deformation mechanisms (Stünitz, 1998). Indeed, the scale of fluid circulation and mass transfer through rocks is mainly controlled by the size and connectivity of the deformation structures, and their evolution through time (Fisher et al., 1995). The permeability of high-pressure rocks being low and fluid pressure close to lithostatic (Etheridge, 1983), most rocks may behave as almost closed-systems, experiencing only small-scale (mm–dm) diffusive mass transfer through the pervasive fluid produced locally by dehydration reactions (Cartwright and Buick, 2000; Fisher et al., 1995; Garofalo, 2012; Spandler et al., 2011; Verlaguet et al., 2011). In these rocks, fluid flow may be channelized in highly deformed zones (shear zones, faults), which form localized preferential pathways for large-scale (m–km) advective mass transfer; open-system fluid–rock interactions are restricted to mm–m scale halos in the surrounding rocks (Abart et al., 2002; Badertscher et al., 2002; Burkhard et al., 1992; John et al., 2012; Li et al., 2013; McCaig et al., 1995, 2000a,b).

However, it is still unclear how open systems develop in previously closed-system rocks and what are the transitional stages. Yet these stages are keys for understanding the fluid system evolution and constraining the (early) rheological evolution of the continental crust when it is subducted or underthrusted. It is therefore a major issue to characterize the fluid system(s) at that time, i.e., the fluid source, the

* Corresponding author at: Université Pierre et Marie Curie, ISTeP, UMR 7193 UPMC-CNRS, Case 129 T46-0, 2ème étage, 4 place Jussieu, 75252 Paris Cedex 05, France. Tel.: +33 1 44 27 71 81; fax: +33 1 27 50 85.
E-mail address: Alexandre.boutoux@upmc.fr (A. Boutoux).

http://dx.doi.org/10.1016/j.lithos.2014.07.005
0024-4937/

circulation timescale and pathways, the intensity of fluid–rock interactions along pathways, as well as the evolution of the fluid system with progressive deformation, especially during the early stages.

Such a study has been performed in the External Crystalline Massifs (ECM) of the external Western Alps. During the Alpine collision phase, this proximal part of the European passive margin was buried to mid-crustal depth below the internal Alpine units at Oligo-Miocene times (Bellahsen et al., 2012; Rolland et al., 2008; Simon-Labric et al., 2009). The ECM experienced mainly thick-skinned deformation during collision: shortening was accommodated by hundred meter-wide shear zones in the basement, while the overlying sedimentary cover was disharmonically folded (Bellahsen et al., 2012; Bellanger et al., 2014; Boutoux et al., 2014). In the northern ECM, i.e., the Mont-Blanc and Aar–Gothard massifs (Fig. 1), the fluid system in the sedimentary cover nappes remained closed to external fluid infiltration, even in highly cleaved metasediments (e.g., Kirschner et al., 1995, 1999; Marquer and Burkhard, 1992). However, the major cover thrusts or mylonites and associated veins record the infiltration of important amounts of basement-derived fluids (Burkhard and Kerrich, 1988; Kirschner et al., 1995, 1999; Marquer and Burkhard, 1992). Indeed, the major basement shear zones propagated as thrusts into the cover, resulting in local opening of the fluid system: ascendant fluids were then channelized within the thrust zones and flowed through both basement and cover (Marquer and Burkhard, 1992; Rolland et al., 2003). Further North, in the Glarus thrust, a localized fluid flow occurred at the basal contact of the sedimentary nappes, as attested by a clear isotopic front due to northward metamorphic fluid flow (Badertscher et al., 2002).

Was the fluid evolution similar in the southern ECM (i.e., North Oisans), which underwent less burial and shortening? In the north-eastern part of the northern Oisans massif (Fig. 1), the cover is locally detached from its basement, which is consequently not involved in crustal shortening (i.e., local thin-skinned tectonic style; Bellahsen et al., 2012). There, cover rocks behaved as a closed-system during the whole deformation process; fluid circulations were restricted to the sedimentary unit scale (Henry et al., 1996). On the contrary, the north-western part of the Oisans massif is characterized by thick-skinned deformation (Bellahsen et al., 2012). However, basement shear zones did not propagate into the cover. Each of these structures having accommodated an amount of shortening of only a few hundred meters they are most likely key features on which one can study the early fluid circulations and probably the transition from closed to open fluid system.

The questions we address in this contribution are the following: what is the scale of the fluid system and its evolution with progressive deformation? As the basement shear bands did not propagate into the cover, how is the deep fluid circulation (if any) accommodated at the basement–cover interface? Can the fluid system give information about the relative timing of basement and cover shortening during the margin inversion? In order to answer these questions, we combine the structural and microstructural analysis of basement shear zones and the overlying metasedimentary cover in the northern Oisans massif with geochemical and microthermometric investigation of the successive vein filling material and host-rocks.

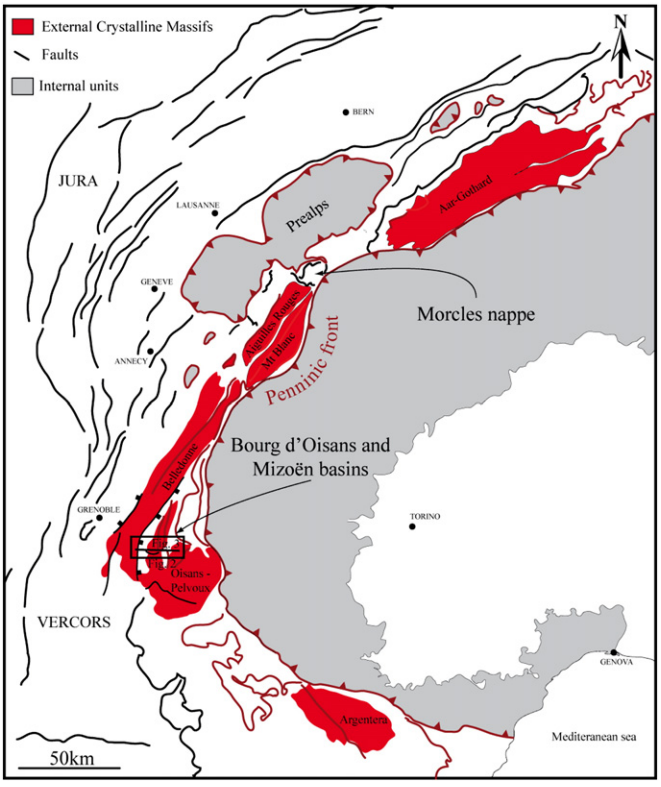

Fig. 1. Schematic structural map of the Western Alps showing the location of the studied area.

2. Geological setting

2.1. The External Alps

The external zone of the Western Alps arc consists of fold-and-thrust belts (Vercors, Chartreuse, Bauges, Bornes, Aravis, Haut Griffre) and External Crystalline Massifs (ECM, Argentera, Oisans, Grandes Rousses, Belledonne, Mont Blanc, Aiguilles Rouges, Aar, Gothard; Fig. 1). It corresponds to the proximal part of the European margin, thinned during Liassic to Dogger times, with the formation of tilted blocks (Lemoine et al., 1989) limited by normal faults oriented N–S to NE–SW in the ECM (Figs. 1, 2).

During the collisional phase of the Alpine orogeny, the ECM were buried down to mid-crustal depth below the internal (Penninic) units. The ECM burial was deeper in the North (400 °C, 5 kbar in the Mont Blanc massif; Rolland et al., 2003; Rossi et al., 2005; 450 °C, 6 kbar in the Aar massif; Challandes et al., 2008) than in the South (270–360 °C and 2–5 kbar in the Oisans massif; Bellanger, 2013; Crouzet et al., 2001; Jullien and Goffé, 1993; Poty et al., 1974).

During collision, basement shortening was accommodated by West-verging reverse shear zones (e.g., Bellahsen et al., 2012; Bellanger et al., 2014; Leloup et al., 2005; Rolland et al., 2008) or anastomosed steep shear zones (e.g., Marquer et al., 2006; Rolland et al., 2008; Oliot et al., 2010, 2014). In the northern Oisans area, the cover was mainly disharmonically folded over basement West-verging shear zones, without significant décollement between the basement and its sedimentary cover (Fig. 3). The main difference between the northern and the southern ECM is that, in the North (Mont Blanc, Aar), basement shear zones propagated into the cover, while in the South (Oisans) shear zones were restricted to the basement and did not propagate into the cover. Moreover, basement shear zones and the associated significant crustal shortening are mainly observed in inverted pre-orogenic Liassic basins (Bellahsen et al., 2012). On the contrary, where the crust was not pre-structured by Liassic extensional basins (e.g., La Grave area in the north-eastern Oisans; Figs. 2, 3), there is less field evidence of significant crustal East–West shortening in the basement, and the cover is detached from the basement, i.e., the shortening style is locally thin-skinned. A striking point in all the basins is the absence of any significant reactivation of the inherited normal faults (Bellahsen et al., 2012; Tricart and Lemoine, 1986).

2.2. Bourg d'Oisans and Mizoën basins

The Bourg d'Oisans and Mizoën basins are pre-orogenic Liassic–Dogger N–S extensional basins bounded by East-dipping normal faults,

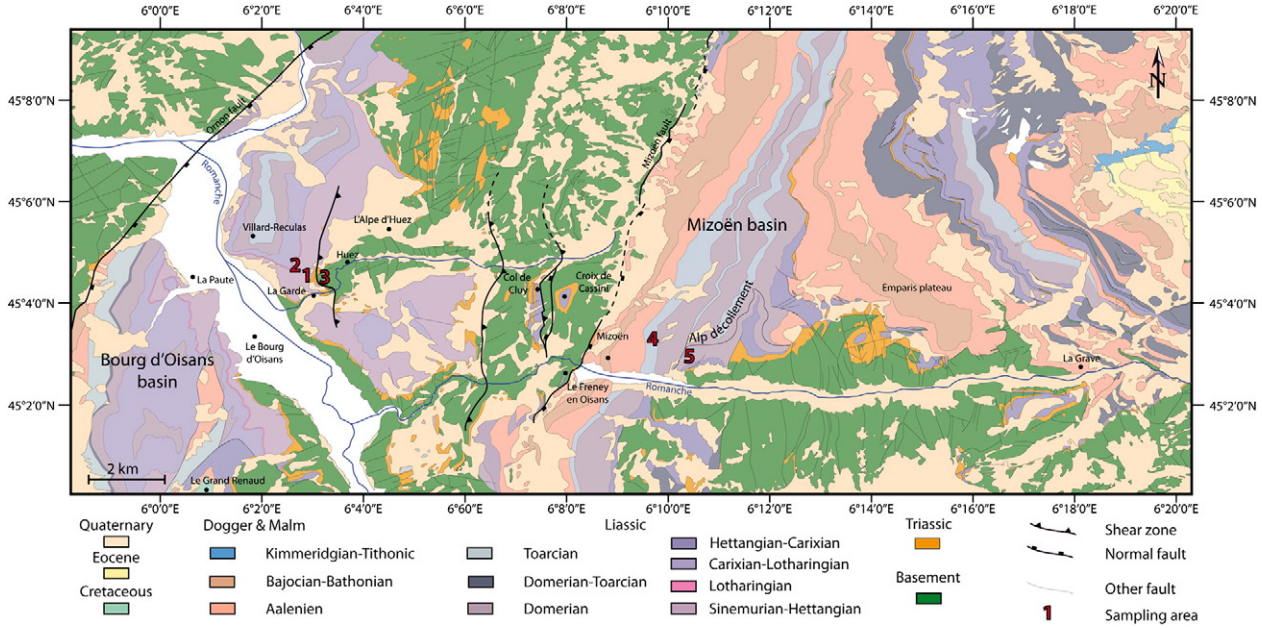

Fig. 2. Geological map of Bourg d'Oisans and Mizoën basins and sampling area location (inset Fig. 1). Modified after Barféty et al. (1972) and Barbier et al. (1973).

the Col d'Ornon and the Mizoën faults, respectively (Figs. 2, 3). Their normal offset values were of 3 and 2.5 km, respectively (Lemoine et al., 1981). The base of the sedimentary cover is composed of a thin Triassic layer (few tens of m) of sandstones and dolomites with scarce gypsum lenses (Figs. 2, 3; Barbier et al., 1973; Barféty et al., 1972). The Bourg d'Oisans basin underwent important subsidence during Liassic (Sinemurian) to Dogger (Bajocian) times, which resulted in the deposition of thick marls or marly limestones. The Mizoën basin was also filled with marls and shales but mainly during Domerian to Bajocian subsidence (Figs. 2, 3).

2.3. Fluid flow in the ECM

In the northern ECM (Mont Blanc and Aar massifs), most studies so far concluded that Alpine fluids were channelized in the major basement and cover shear zones (Badertscher et al., 2002; Kirschner et al., 1999; Marquer and Burkhard, 1992; Rolland et al., 2003; Rossi et al., 2005). Indeed, at the proximity of large thrusts (i.e., within a few meters), oxygen isotopic values ($\delta^{18}O$) in shear zones and associated veins are locally much lower than in the surrounding rocks within the cover nappes (e.g., Badertscher et al., 2002; Burkhard and Kerrich,

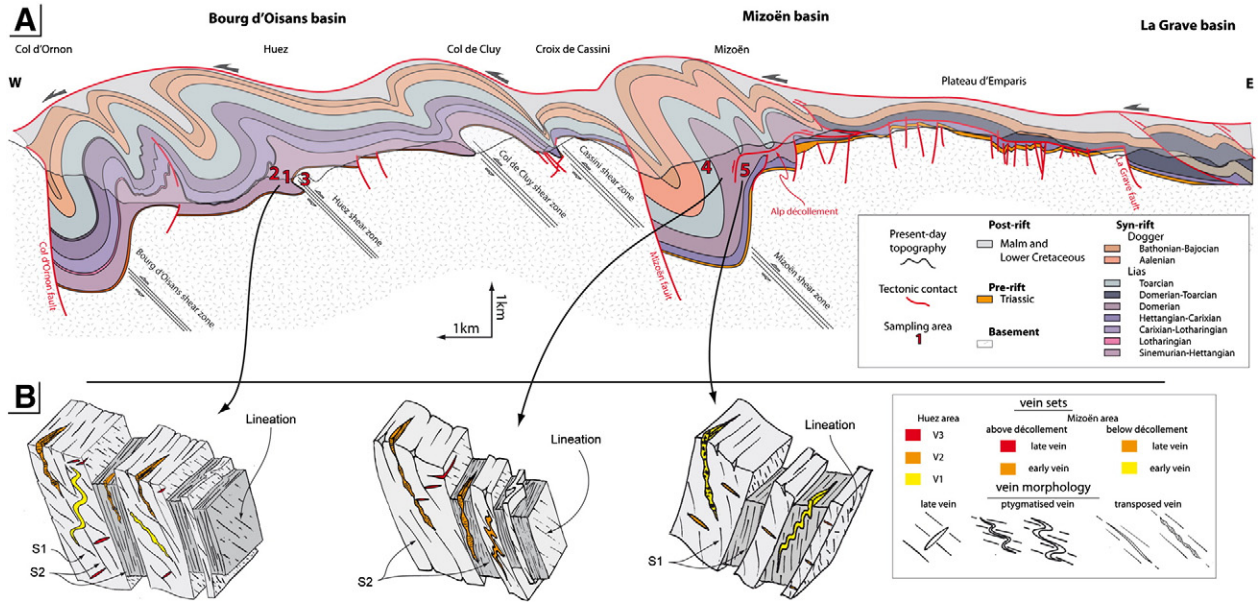

Fig. 3. Cross-section of Bourg d'Oisans and Mizoën basins and sketch of metamorphic vein formation. A. Cross-section of Bourg d'Oisans and Mizoën basins showing sample locations, modified after Boutoux et al. (2014). The basement is locally sheared while the overlying cover is disharmonically folded. B. 3D schematic representation of the vein sets relative chronology and their relationships with the cleavages.

1988; Marquer and Burkhard, 1992), which is interpreted as the result of large-scale fluid flow from deeper (basement) parts of the shear zones. However, apart from the basal thrusts of the largest nappes, similar values of oxygen isotopic compositions ($\delta^{18}O$) were observed in the cover shear zones and the surrounding rocks within the nappes (Kirschner et al., 1999), suggesting that these rocks underwent little to no advection of isotopically distinct fluid.

In the southern ECM and especially in the Oisans area, few geochemical studies have been performed and none of them provided any evidence of large-scale fluid circulation. In particular, Henry et al. (1996) carried out a geochemical study of the metasedimentary rocks of La Grave (Fig. 2), where the cover is detached from its probably undeformed underlying basement (Bellahsen et al., 2012). Isotopic and trace element signatures of metamorphic vein filling material and their host-rocks show that the metasedimentary cover behaved as a chemically closed-system, locally-derived fluid circulations being restricted to the metasedimentary Jurassic units (i.e., few tens of meter scale; Henry et al., 1996).

Microthermometric studies all over the Bourg d'Oisans basin carried out on fluid inclusions trapped within vein mineral phases also suggest the absence of large-scale fluid circulation in the Oisans Jurassic cover, although high salinities recorded in some fluid inclusions in the deeper Liassic layers were interpreted as due to a local percolation of fluids from the underlying Triassic gypsum (Bernard, 1978; Gratier and Vialon, 1980; Gratier et al., 1973; Nziengui, 1993; Poty et al., 1974).

3. Large-scale structures and microstructures

3.1. Large-scale structures

In both the Bourg d'Oisans and Mizoën basins, basement shortening was accommodated by West-verging 100–500 m wide shear zones (Bellanger et al., 2014) restricted to the basement (i.e., they did not propagate significantly into the cover) and that cut across the Variscan foliation (Fig. 3A), without any evidence for its reactivation. The two basins have slightly different styles of shortening. In the Bourg d'Oisans basin, there are five units (Dumont et al., 2008) that are separated by four West-verging shear zones named Bourg d'Oisans, Huez, Col de Cluy, and Croix de Cassini shear zones (Fig. 3A). Above these basement shear zones, the sedimentary cover is disharmonically folded. The observed meter-to-kilometer scale fold axes are N–S and synchronous with the main cleavage. The Mizoën basin is divided into two parts: the eastern part is a basement horst named the Emparis Plateau, with a thin metasedimentary cover (Figs. 2, 3A), whereas the western part is composed of a thicker disharmonically folded metasedimentary cover (Fig. 3A) underlain by the main West-verging basement shear zone (the Mizoën shear zone). Just West of the Emparis Plateau, the Mizoën metasedimentary cover is composed of two structural units separated by the Alp décollement (Fig. 3A). Note that the base of the sedimentary cover is composed of a thin Triassic layer (a few tens of meters wide) attached to the basement, i.e., not disharmonically folded.

3.2. Cleavages in the sedimentary cover

Several cleavages affecting the metasedimentary cover are documented in the field (Bellahsen et al., 2012; Boutoux et al., 2014; Dumont et al., 2008, 2012). In the Bourg d'Oisans basin, one main cleavage (S2) is observed (Figs. 3, 4A–B), striking N–S and dipping eastward. This cleavage is associated with the main folds whose axial surface is East-dipping (Gratier and Vialon, 1980; Gratier et al., 1973). Close to the basement of the Bourg d'Oisans basin, a previous cleavage (S1) can also be documented (Fig. 3B), striking N–S and dipping westward. The chronological relationships between the two cleavage sets are described in Bellahsen et al. (2012) and Boutoux et al. (2014): during the initiation of the basin inversion, the base of the sedimentary cover underwent a top-to-the-East shearing that locally formed the West-dipping S1 cleavage. This cleavage was then overprinted by the S2 main cleavage resulting from the top-to-the-West shearing of the entire basin (Fig. 3). In the Mizoën basin, the S1 cleavage is only recorded below the Alp décollement, while the S2 cleavage developed only above it (Figs. 3, 4C–D).

3.3. Vein pattern and sequence

During the development of the two cleavages, metamorphic veins were continuously formed and deformed in the metasedimentary cover. Vein deformation occurred either by transposition into cleavage or by folding (i.e., ptygmatic vein; Fig. 4). In the field, three successive vein sets could be distinguished owing to their crosscutting relationships with S1 and S2 cleavages (Boutoux et al., 2014). V1 veins were deformed by both cleavages (Fig. 4C), V2 veins cut across S1 but were deformed by S2 cleavage (Fig. 4A), and V3 veins are undeformed and cut across both cleavages (Fig. 4B). V1 veins are interpreted as pre- to syn-S1 cleavage, V2 veins as pre- to syn-S2 cleavage and V3 veins as late- to post-S2 cleavage. Indeed, most V3 veins are perpendicular to S2 but undeformed, therefore compatible with the end of the ductile event forming the S2 cleavage. Therefore, most of the veins are related to the main ductile deformation event associated to the development of S1 and S2 cleavages (Boutoux et al., 2014), except the latest V3 veins that can be related to the basin exhumation.

Locally, where only one cleavage is expressed, only two vein generations can be distinguished, e.g., far from the basement in both basins, where S1 and S2 cannot be distinguished. In this case, V1 and V2 veins cannot be discriminated and are labeled as "early veins" (Fig. 4B–D). Moreover, under the Alp décollement in the Mizoën basin, where S1 only is expressed, V2 and V3 veins are undistinguishable and considered as "late veins". The structural relationships between vein sets and cleavages are summarized in Fig. 3B.

4. Sampling strategy and analytical techniques

In order to investigate the scale of fluid circulation in the metasedimentary cover rocks in the Bourg d'Oisans basin and to identify potential basement-derived fluid infiltration, we collected samples in the Huez basement shear zone and in the cover right above, at different distances above the basement–cover interface (Fig. 3). Basement samples from the Huez shear zone itself were sampled on the road between La Garde and l'Alpe d'Huez, a few meters under the basement–cover contact (location 3 in Figs. 2, 3A), along with Triassic samples. Cover samples were collected in two places: (1) a few tens of meters above the basement–cover contact on the road between La Garde and l'Alpe d'Huez (called "Huez samples" thereafter; location 1 in Figs. 2, 3A) and (2) about 300 m structurally higher, on the road between Huez and Villard-Reculas (called "Villard-Reculas samples" in this study; location 2 in Figs. 2, 3A).

We also collected samples from the cover in the Mizoën basin, between the Mizoën village and the Emparis plateau, from both tectonic units separated by the Alp décollement, i.e., above (location 4 in Figs. 2, 3A) and below it (location 5 in Figs. 2, 3A), in order to investigate the possible effect of this tectonic contact on potential fluid circulations. Unfortunately, the underlying basement shear zone could not be sampled, because (1) it does not crop out around the Romanche valley (Fig. 3A) and (2) further South, in the Veneon valley, the sheared basement is accessible, but according to Barbier et al. (1973), the lithology is quite different than in the Romanche valley.

Most analyses were performed at ISTeP (Paris, France), except when specified in the following. Whole-rock analyses were performed at the SARM (Nancy, France) on six representative cover and basement samples from the Huez area (locations 1, 2, and 3 in Figs. 2, 3A). The vein and host-rock mineralogy was determined by X-ray diffraction (D2 Phaser Bruker) and EDS analyses (SDD detector PGT Sahara) associated to scanning electron microscopy (SEM Zeiss Supra 55VP). Cover vein

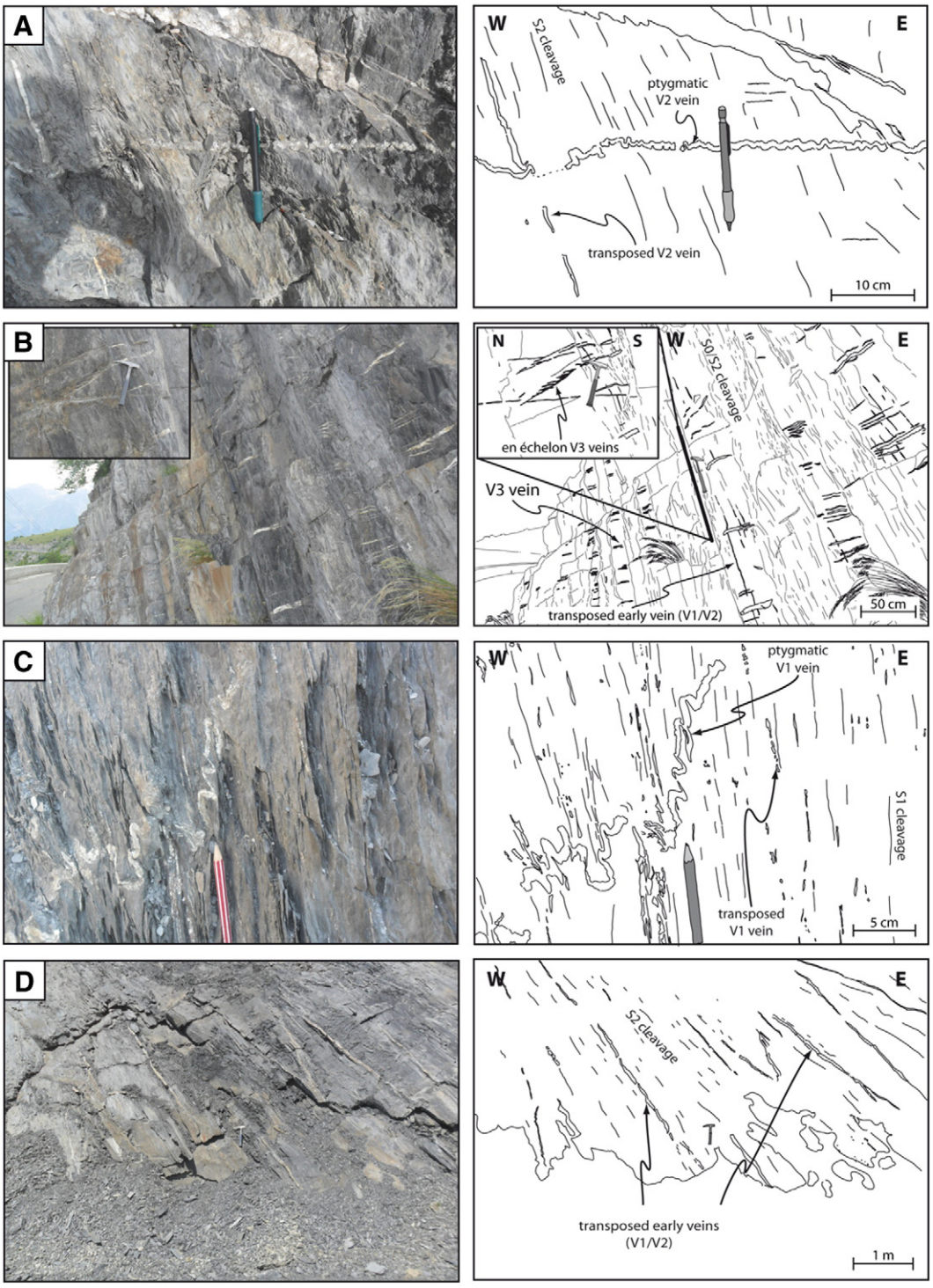

Fig. 4. Successive metamorphic veins and their chronological relationships with the cleavage sets in cover rocks from Bourg d'Oisans and Mizoën basins, microphotographs and schematic interpretation. A–B: Bourg d'Oisans basin (location 2 in Figs. 2, 3A). A. Transposed V2 vein into the S2 cleavage and folded (ptygmatic) V2 vein with S2 cleavage as fold axial plane. B. Late V3 veins, sometimes en-échelon, crosscutting the S2 cleavage in pelitic-rich layers. C. Mizoën basin, below the Alp décollement (location 5 in Figs. 2, 3A). V1 vein transposed into S1 cleavage and ptygmatic V1 vein with S1 cleavage as fold axial plane. D. Mizoën basin, above the Alp décollement (location 4 in Figs. 2, 3A). Early veins (V1 or V2) transposed into S2 cleavage.

microstructures were characterized under SEM and optical microscope. Cathodoluminescence (Cathodyne OPEA) on cover veins and host-rocks was used to identify successive crystallization generations. To investigate local versus external fluid infiltration in metasedimentary cover rocks, the isotopic signature ($\delta^{13}C$, VPDB and $\delta^{18}O$, SMOW) of vein calcite was compared to that of their surrounding host-rocks. The $\delta^{18}O$ of quartz (laser fluorination at IPGP, Paris, France) and calcite in textural equilibrium in the different vein sets were combined in order to constrain the fluid temperature during vein mineral crystallization. Trace element analyses were performed (ICP-MS, following the methodology of Salaün et al., 2010) on the different vein sets and their host-rocks, and on samples from the underlying basement (for the Huez shear zone) in order to detect any basement-derived fluid infiltration into cover rocks. Besides, microthermometric measurements were performed on primary fluid inclusions in quartz and calcite from Huez and Mizoën (locations 1 and 5 in Figs. 2, 3A, respectively) cover veins,

providing fluid salinity and isochoric evolution paths. Finally, the combination of calculated isochors and quartz–calcite equilibrium temperature provided fluid pressure estimates during the vein formation. More details about the analytical procedures can be found in Appendix A.1.

5. Mineralogy and textures of basement and cover rocks and veins

5.1. Mineralogy of basement rocks

In the Bourg d'Oisans basin, the Huez Alpine shear zone (location 3 in Figs. 2, 3A) presents a thick talc-rich zone of a few meters width. This talc-rich zone is composed of rocks with very mafic Ca-rich composition (Table 1) exhibiting the following minerals: talc, Cr-rich chlorite, Mg–Ca-amphibole, plagioclase, Ni-rich pyrite, sphene, chromite, rutile and titanomagnetite (Fig. 5). Talc, chlorite and sphene are observed to have co-crystallized in shear zones, where they clearly replace amphibole (Fig. 5A) and plagioclase. Pyrite cores included in amphibole crystals are rimed by iron-oxide or hydroxide (Fig. 5B), which formation is associated and coeval with talc crystallization in cracks through the amphibole crystals. Zoned chromite crystals are partly dissolved and embedded in Cr-rich chlorite (Fig. 5C, D, E). These mineralogical reactions required both rock hydration (to form phyllosilicates) and progressive evolution towards more oxidizing conditions (i.e., pyrite rims).

Therefore, two successive parageneses can be identified: (1) the assemblage amphibole + plagioclase + pyrite + chromite + rutile corresponds to the Variscan paragenesis also observed by Barféty et al. (1972) in the unsheared basement and is in agreement with description by Guillot and Ménot (2009), and (2) the assemblage talc + chlorite + sphene + Fe-oxide/hydroxide + titanomagnetite is obviously related to basement shearing, accompanied by external fluid influx, during the Alpine collision. Indeed, this second paragenesis grew in Alpine shear zones, and the presence of chlorite is characteristic of the greenschist facies P–T conditions undergone by basement rocks during the Alpine collision.

In the talc zone, numerous quartz veins and scarce calcite veins (e.g., sample Alp10-5 in the following results) are kinematically consistent with Alpine shearing, and thus considered of Alpine age.

5.2. Mineralogy of cover rocks

The Triassic layers, still attached to the basement rocks, are mainly composed of sandstone, dolomite and scarce lenses of gypsum (Table 1). Above the Huez basement shear zone, fractures in the Triassic layers are mainly filled with calcite, dolomite and quartz, with local enrichments in galena (PbS), pyrite (FeS_2) and/or sphalerite (ZnS). These minerals can be locally concentrated, e.g., in the La Gardette (Cathelineau et al., 1990; Marignac et al., 1997; Poty, 1967) and Le Pontet (Feybesse et al., 2004) ancient gold mines: these sulfur minerals crystallized in a 500 meter long quartz vein affecting both the basement (granite and gneiss) and the lowermost Triassic dolomites. In La Gardette, similar sulfur minerals are also concentrated in a specific level of the Triassic dolomite, where they were interpreted as syn-sedimentary enrichments (Poty, 1967).

In both the Huez and Mizoën basins, the metasedimentary cover is made of marls (Table 1) containing calcite, quartz, phyllosilicates (mainly pyrophyllite, chlorite, phengite and rare cookeite), iron oxides, rutile, and pyrite (Fig. 6A–B). Framboidal pyrite is observed and is interpreted as formed during early diagenesis (Wilkin et al., 1996). The pyrites are often partially to completely oxidized (Fig. 6A). Detrital albite grains and rare dolomite (Fig. 6B) and apatite crystals were also observed. The phyllosilicate paragenesis is characteristic of the Alpine greenschist facies metamorphism. The analyzed samples (Table 1) show a large compositional variability, which results in variable proportions of calcite (30–90 vol.%) versus quartz (0–20 vol.%), phyllosilicate fraction (5–40 vol.%) and organic matter (0.5–1.5 wt.%; modal composition calculations according to Verlaguet et al., 2011).

Finally, host-rocks show calcite dissolution zones (Fig. 6A), attesting material displacement by pressure-solution into the sedimentary cover.

5.3. Textures and mineralogy of veins

In both basins, veins are mainly filled with calcite and quartz, the quartz amount decreasing from V1 to V3, so that many V3 veins are devoid of quartz and only filled with calcite. Calcite and quartz display either fibrous crystals elongated perpendicular to the vein walls ("fibrous texture" in the classification of Oliver and Bons, 2001; Fig. 6C) or euhedral morphologies ("blocky texture" in Oliver and Bons, 2001; Fig. 6C, D, E), whatever the vein generation. Both textures can coexist in synchronous veins in the same thin section (e.g., late veins in Fig. 6C), and mixed textures are also observed.

Quartz and calcite crystals show multiple evidences of textural equilibrium: they often show mutual micro-indentations (intergrowth textures), and some calcite crystals are embedded within quartz crystals, themselves surrounded by calcite crystals of similar composition (Fig. 6F). The textural equilibrium of calcite and quartz in veins indicates their co-precipitation.

Scarce accessory micrometric phases such as dolomite, apatite, oxidized pyrite and chlorite can be recognized with SEM.

Table 1
Chemical analysis (wt.%) of Bourg d'Oisans basin cover and basement rocks.

Sample	Alp10-8[a]	Alp10-13[a]	Alp 10-34[b]	Alp10-II-15[a]	Alp10-II-16[a]	Alp10-3[c]
Sample location	1	1	1	2	2	3
SiO_2	40.38	23.02	2.17	4.88	32.45	34.84
Al_2O_3	14.21	6.04	0.53	2.84	8.55	0.79
$Fe_2O_{3\ total}$	3.16	2.41	2.51	1.1	3.52	4.78
MnO	0.04	0.04	0.37	0.25	0.37	0.39
MgO	3.34	4.3	19.13	1.24	3.13	26.38
CaO	15.42	30.57	30.06	47.93	24.25	12.38
Na_2O	0.35	0.51	0.26	0.15	0.56	–
K_2O	4.01	1.20	0.07	0.55	1.69	–
TiO_2	0.57	0.31	0.03	0.12	0.41	0.02
P_2O_5	0.17	0.18	–	0.06	0.17	–
L.O.I.	17.83	30.04	43.79	39.49	24.13	21.08
Total	99.48	98.63	98.92	98.62	99.24	100.67
$CO_{2\ total}$	16.85	31.76	44.77	39.78	23.34	18.38
$H_2O_{\ total}$	2.87	1.67	0.73	1.23	2.22	3.45

L.O.I., loss on ignition. Whole-rock chemical analysis (oxide weight %).
[a] Jurassic.
[b] Triassic.
[c] Sheared basement.

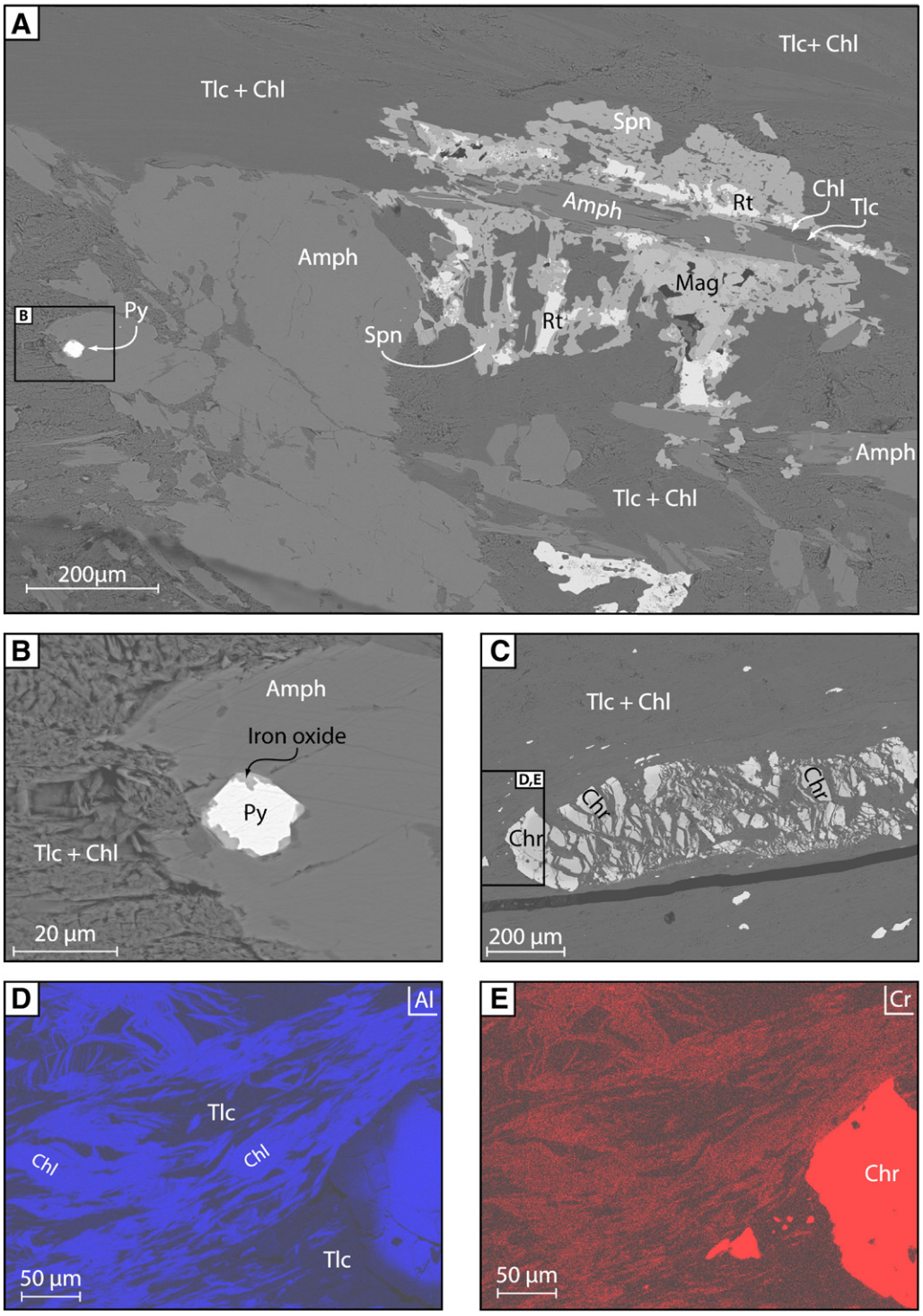

Fig. 5. Thin section of the Huez talc-rich basement shear zone (sampling location 3 in Figs. 2, 3A). BSE-SEM images. A. Hercynian paragenesis amphibole (Amph) + pyrite (Py) + rutile (Rt) partially replaced by the Alpine assemblage talc (Tlc) + chlorite (Chl) + sphene (Spn) + titanomagnetite (Mag). B. Ni-rich pyrite included in Hercynian amphibole is altered into iron-oxide rims by fluid ingression into amphibole cracks during the Alpine shearing, as attested by the coeval retrogression of amphibole into talc + chlorite. C. Hercynian chromite (Chr) partially dissolved and replaced by talc + chlorite. D–E Elementary maps (EDS-SEM analysis) of AlO (D) and CrO (E), showing that the Alpine chlorite locally incorporates part of the chromium liberated by the Hercynian chromite dissolution (mineral abbreviations following Kretz, 1983).

6. Geochemical signatures and microthermometry of veins and host-rocks

6.1. Cathodoluminescence microscopy

Several samples from the three vein generations (from both the Bourg d'Oisans and Mizoën basins, locations 1–2 and 4–5 in Figs. 2–3A, respectively) were analyzed under cathodoluminescence. Two representative V1 and V2 veins are illustrated in Fig. 6G–H. In V1, V2 and their host-rock, calcite displays the same red color, with the same intensity (Fig. 6H). Quartz in V1 vein and other phyllosilicate phases in the host-rock appear in black and lighter red, respectively (Fig. 6H), as they do not incorporate the same amount of luminescent elements. A similar red color was observed in V3 veins and their host-rocks on other samples.

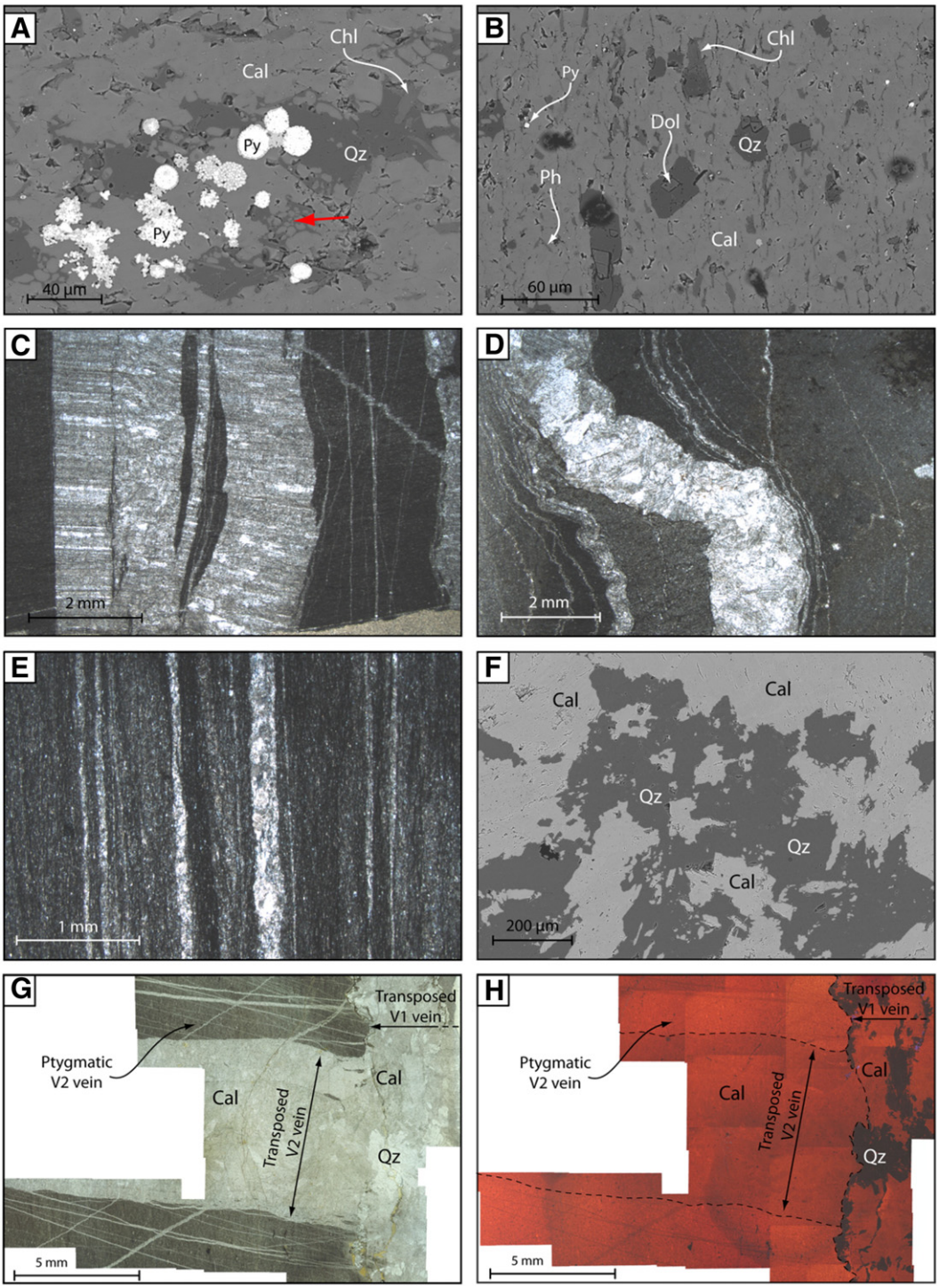

Fig. 6. Thin-sections of cover veins and their host-rocks. SE-SEM images (A, B), photomicrographs in natural light (C, D, E, F) and under cathodoluminescence (H). A. Calcite (Cal), quartz (Qz), chlorite (Chl), and framboidal pyrite (Py) observed within cover host-rock thin section. Pyrite cores are partly oxidized. The arrow highlights a calcite dissolution zone within the host-rock. B. Host-rock mineralogical assemblage composed of calcite, quartz, phengite (Ph), chlorite, framboidal pyrites and scarce dolomite (Dol). C. Late V3 veins (calcite + quartz) showing either blocky or fibrous texture, crosscuting V2 ptygmatic vein. D. Ptygmatic V1 veins with blocky textures. E. Transposed V2 veins with blocky textures. F. Calcite and quartz in textural equilibrium (micro-indentation) in V1 vein: calcite is included in quartz crystals, which are embedded in calcite crystals. G–H. Thin section of cover veins from sample Alp10-20 (location 1 in Figs. 2, 3A) observed under natural light (G) and cathodoluminescence (H). Sample showing two vein generations: V1 transposed into S1 cleavage, and numerous V2 (only the major one is underlined) transposed into S2 cleavage and crosscutting V1. V1 contains quartz + calcite + scarce apatite, while V2 is filled with calcite only. Mineral abbreviations following Kretz (1983).

These observations indicate that the nature and concentration of luminescent elements incorporated in calcite did not vary during the successive vein crystallization, and are similar to that of the host-rock calcite. In these samples, calcite appears red although pure calcite is usually orange under cathodoluminescence microscopy (Machel and Burton, 1991): this may indicate a high concentration in red luminescent elements such as manganese or magnesium.

The absence of variation in either color or intensity of calcite within the veins precludes any evidence of successive growing phase in any vein generation.

6.2. $\delta^{18}O$ and $\delta^{13}C$ signatures of calcite from veins and host-rocks

$\delta^{18}O$ and $\delta^{13}C$ signatures of calcite from cover veins and their host-rocks from both basins (sample locations 1, 2, 4, and 5 in Figs. 2, 3) along with one calcite vein from the talc-rich zone of the Huez basement shear zone (sample location 3 in Figs. 2, 3) are reported in Fig. 7A. In the Bourg d'Oisans basin, the isotopic ratios, whatever the vein generation, are very close to that of their host-rock (Fig. 7B–C). $\delta^{18}O$ and $\delta^{13}C$ composition ranges of most veins and host-rocks are relatively narrow: +18 to +23.5‰ and −2 to +1.5‰, respectively (Fig. 7A). These variations mainly reflect lithological variations: the most pelitic (i.e., phyllosilicate-rich) samples exhibit the lowest $\delta^{18}O$ and $\delta^{13}C$ signatures. In the Mizoën basin, the isotopic signatures of each vein are also very close to those of their host-rocks (Fig. 7B–C). Two groups can be identified: one group has isotopic composition within the range of Bourg d'Oisans rocks ($\delta^{18}O = +21.5$ to +23.5‰, $\delta^{13}C = -1$ to +1.5‰, Fig. 7A), while the second group has lower $\delta^{18}O$ (+19.5 to +21.5‰) and $\delta^{13}C$ (−2.5‰ to −6‰, Fig. 7A). This bimodal distribution is correlated to the rock lithology: all samples with negative $\delta^{13}C$ (pelitic layers on Fig. 7A) belong to the Aalenian layer, which is particularly rich in phyllosilicates and organic matter, while other compositions correspond to samples collected in marls.

Cover vein and host-rock calcite presents very homogeneous isotopic signatures (Fig. 7B–C). On the contrary, the isotopic signature of the calcite vein from the Huez basement shear zone shows a strikingly different value ($\delta^{13}C = -9.2$‰ and $\delta^{18}O = +13.3$‰, Fig. 7A) compared to the cover vein calcite. In the Triassic layer, the isotopic composition of the vein ($\delta^{13}C = -5.3$‰, $\delta^{18}O = +19.5$‰) is very different from that of its host-rock ($\delta^{13}C = -1.5$‰, $\delta^{18}O = +25.7$‰, Fig. 7A), and intermediate between Triassic host-rock and basement vein composition (Fig. 7A).

6.3. $\delta^{18}O$ signatures of quartz from cover veins

The $\delta^{18}O$ signatures of quartz crystals in textural equilibrium with calcite in cover veins from both basins (sample locations 1, 2, 4, and 5 in Figs. 2, 3A) are relatively homogeneous for most veins ($\delta^{18}O = +22.3$ to +26.3‰, Table 2) whatever the sampling site or vein generation.

6.4. Microthermometric study of fluid inclusions in veins

Microthermometric measurements were performed on about 80 fluid inclusions in either quartz or calcite crystals from V1 or early (V1/V2) cover veins from both basins (locations 1 and 5 in Figs. 2, 3). In order to characterize the fluid phase present in cover veins during mineral crystallization, we focused on primary fluid inclusions, which are interpreted as being trapped during crystal growth (Roedder, 1984; Touret and Frezzotti, 2003). Primary fluid inclusions are distributed either in trails along successive crystal growth surfaces (Fig. 8A) or in clusters (Fig. 8B) throughout the vein crystals (Roedder, 1984). In veins showing fibrous textures, we also analyzed the pseudo-secondary trails of fluid inclusions (Fig. 8C, D).

For each fluid inclusion, the salinity of the fluid was calculated from the measured melting temperature (Tm) with the equation presented in Bodnar (1993). Measured Tm is between −1 °C and −10 °C (dispersion of ±3 °C for each sample), which corresponds to 1.74wt.% eq. NaCl and 13.94wt.% eq. NaCl, respectively. Measured homogenization temperatures (Th) are between 125 °C and 198 °C (dispersion of ±12 °C in a single sample). Then, isochoric P–T relationships were calculated for each sample from the mean measured Th and mean calculated salinity, using the equation of Bodnar and Vityk (1994). The isochors (Fig. 9) are almost parallel, with P–T relationships of 16.5 MPa·C^{-1} to 21 MPa·C^{-1}, whatever the basin (Bourg d'Oisans or Mizoën).

6.5. Trace element analysis in veins and host-rocks

For both basement and cover rocks, trace element concentrations of 3d transition elements (Sc, V, Cr, Co, Ni, Cu and Zn) and HFSE (Zr, Hf, Nb, Ta, Mo, Sb) were normalized to mean crust composition (Taylor and McLennan, 1985; Fig. 10A, B) to allow comparison. However, basement rocks have Ca-rich basic compositions, and cover rocks are Triassic

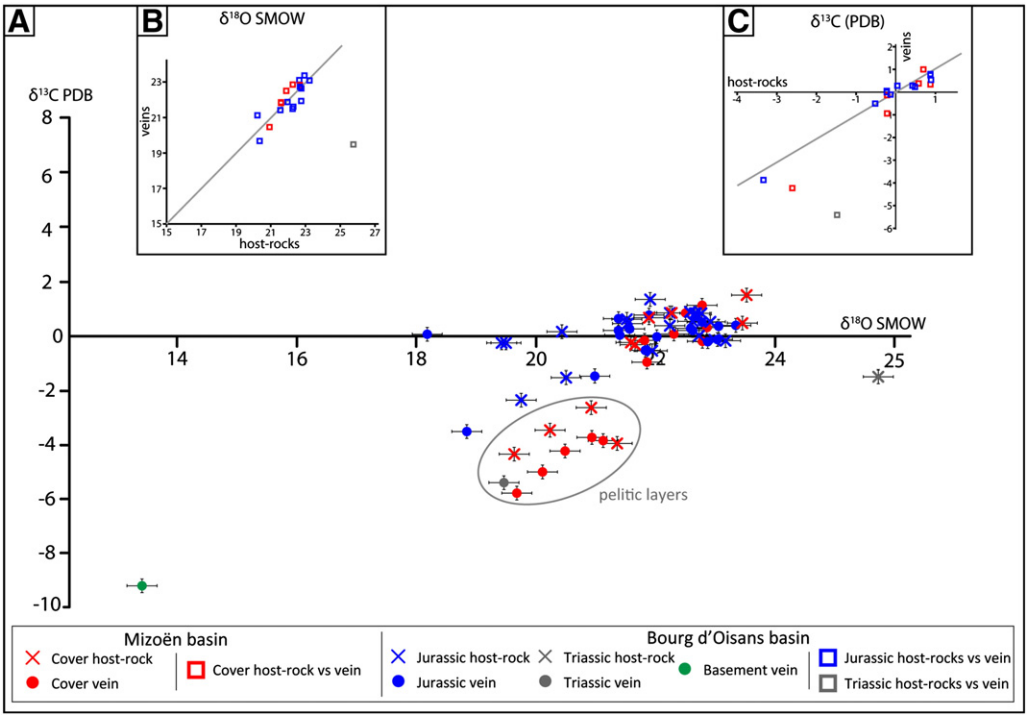

Fig. 7. Stable isotopic ratios ($\delta^{18}O$ and $\delta^{13}C$) of calcite from vein and host-rock samples in Bourg d'Oisans (locations 1 and 2 in Figs. 2, 3A) and Mizoën (locations 4 and 5 in Figs. 2, 3A) basins. A. $\delta^{18}O$ versus $\delta^{13}C$ for Jurassic and Triassic calcite. In addition, the isotopic analysis of a calcite vein from the talc-rich zone of the sheared basement shear zone is plotted (location 3 in Fig. 2, 3A). "Pelitic layers" highlights samples from the Aalenian layer, which is particularly phyllosilicate-rich (Barbier et al., 1973). B and C. $\delta^{18}O$ (B) and $\delta^{13}C$ (C) of vein calcite versus their respective host-rock calcite (i.e., for samples where both vein and host-rock calcite was analyzed). Solid line: linear relationship between vein and host-rock isotopic ratios.

Table 2
$\delta^{18}O$ of vein calcite and quartz presenting textural equilibrium (fine micro-indentation, see Fig. 6F).

Sample	Sample location	Quartz $\delta^{18}O$ (‰)	Calcite $\delta^{18}O$ (‰)	T (°C)
Alp10-13[a]	1	25.2	22	251
Alp10-15	1	24.8	21.8	274
Alp10-18	1	24	21.8	358
Alp10-20[a]	1	25.2	23.1	421
Alp10-21	1	25.3	23	344
Alp10-22[a]	1	25.7	21.6	189
Alp10-34	1	24.6	19.5	144
Alp10-II-2	2	24.7	22.2	327
Alp10-II-6[a]	2	26.3	23.5	292
Alp10-II-11	2	25.8	23.2	314
ALp10-52	4	22.3	19.7	306
Alp10-55[b]	4	22.3	20.5	429
Alp10-64[b]	4	23.8	21.9	402
Alp10-74	4	24.6	22.8	417
Alp11-15	5	25.7	23.9	436

$\delta^{18}O$ for quartz and calcite expressed in ‰ SMOW. $\delta^{18}O$ on quartz corrected from standard analysis (UWG2 garnet).
Analytical precision for $\delta^{18}O$ on calcite (0.1‰) and quartz (0.08‰) gives a propagated error on $\Delta^{18}O_{quartz-calcite}$ ($=\delta^{18}O_{quartz} - \delta^{18}O_{calcite}$) of 0.12‰.
Equilibrium quartz–calcite temperatures calculated from Sharp and Kirschner (1994); estimated uncertainty on the thermometer: from ±15 °C to ±26 °C in the 200–450 °C range, systematically higher than the maximum error on the equilibrium temperature calculated from the analytical precision on quartz and calcite $\delta^{18}O$: from ±7 °C to ±22 °C in the 200–450 °C range.
Veins are all V1 veins for Bourg d'Oisans samples (locations 1 and 2 on Figs. 2, 3A) or early veins (undetermined V1 or V2 veins) for Mizoën samples (locations 4 and 5 on Figs. 2, 3A).
[a] Duplicated samples showing a deviation from mean value ≤ ±0.3‰: equilibrium quartz–calcite temperature calculated from the mean $\delta^{18}O$ value.
[b] Samples showing highly dispersed duplicates (±0.6 and 0.9‰): for both samples, the highest $\delta^{18}O$ value gives an unrealistically high equilibrium temperature (863 °C and 3944 °C respectively), exceeding both the thermometer calibration temperature range and the maximum temperature estimated for these rocks (300–350 °C; Bellanger, 2013; Crouzet et al., 2001; Jullien and Goffé, 1993); these unrealistic $\delta^{18}O$ values were discarded, and the equilibrium quartz–calcite temperature was calculated from the valid $\delta^{18}O$ analysis.

dolomites and Liassic marls, thus these rocks display accordingly specific patterns relative to the mean crust composition. As the aim of this study was to trace potential basement-derived fluid infiltration in cover rocks, trace element patterns normalized to mean crust composition are discussed hereinafter in terms of relative variations of shapes rather than in terms of absolute values. The trace element patterns of sheared and unsheared basement, basement and cover rock, and cover vein versus host-rock are also compared. Trace element values can be found in Appendix Table A.2.

6.5.1. Basement trace element patterns

Trace elements were analyzed in samples collected both in the Huez basement shear zone (including the talc-rich area, Fig. 10D) and just outside the shear zone in less deformed rocks.

Basement trace element concentrations are presented on Fig. 10A normalized to the mean crust (Taylor and McLennan, 1985). For most elements, trace element patterns of samples from the sheared basement are similar to those of the unsheared basement with however lower absolute contents, except in Ni, Co and Cr (Fig. 10A). These lower concentrations in sheared basement samples reflect either trace element depletion in basement rocks during shearing or trace element dilution effects due to depletion or enrichment in some major elements.

Concerning the sheared basement, trace element compositions in samples from the shear zone outside of the talc-rich zone follow the same trend than the talc-rich zone samples (Fig. 10A–D), except for the Cr, Co, and Ni concentrations that are clearly higher in the talc-rich zone: Cr, Co, and Ni patterns are even inversely correlated in both zones. This suggests that the shearing of basement rocks has mainly affected the compositions in Cr, Co and Ni, probably through fluid-assisted mobilization, while other 3d transition elements and HFSE (known as the least mobile) remained unaffected.

In the talc-rich shear zone, the calcite vein from sample Alp10-5 has a similar pattern (except in Zn and Mo) than its host-rock, with bulk depletion in all trace elements.

6.5.2. Cover trace element patterns

Trace element concentrations of cover rocks are presented normalized to the mean crust ones (Fig. 10B; Taylor and McLennan, 1985) whereas the vein trace element concentrations are presented normalized to their host-rocks (Fig. 10C).

Composition patterns of Triassic dolomites are slightly enriched in Zn, Mo, and Sb compared to the mean crust composition (Fig. 10B). The associated veins are enriched in Zn ± Sb and V compared to their host-rocks (Fig. 10C).

In Liassic layers above the Huez shear zone, the samples have very similar trace element patterns, whatever their distance to the contact (Fig. 10B): indeed, both Huez (a few tens of meters above the basement, location 1 in Figs. 2, 3, 10D) and Villard-Reculas (a few hundred meters from the basement, location 2 in Figs. 2, 3, 10D) samples exhibit similar concentrations in all elements (Fig. 10B), with higher concentrations in V, Zn, Mo and Sb than mean crust composition (Fig. 10B). The variability of trace element concentrations in marls may reflect their heterogeneous calcite content (30–90 vol.%, Table 1) versus pelitic fraction content.

All the veins sampled just above the Huez basement shear zone (location 1 in Figs. 2, 3A, 10D) present strong enrichments in Ni (up to 100 times) and/or Co (up to 10 times), Cr (up to 10 times), Zr and Hf (up to 100 times) compared to their respective host-rocks (Fig. 10C), for V1, V2 and V3 veins. On the contrary, veins sampled farther from the basement–cover interface (location 2 in Figs. 2, 3A, 10D) display a bulk depletion in all trace elements compared to their host-rocks, and do not present any particular trace element enrichment (Fig. 10C).

7. Interpretation of results and discussion

7.1. Scale of fluid circulation and mass transfer in the metasedimentary cover

7.1.1. Isotopic reequilibration of host-rocks during burial

In samples from the metasedimentary cover of the Bourg d'Oisans and Mizoën basins, calcite shows a homogeneous isotopic composition in each lithological unit (Fig. 7A). However, the calcite isotopic signal is not that of a typical marine limestone, and plots between "normal marine limestones" and "metamarls-metapelites" isotopic values (Fig. 11) reported by Henry et al. (1996). This means that isotopic reequilibration occurred among the different minerals (quartz, calcite, phyllosilicate fraction, organic matter) during burial. Following Henry et al. (1996), we conclude that these cover rocks attained complete isotopic reequilibration under greenschist facies conditions.

As a consequence, the isotopic signature of host-rocks seems to be mainly controlled by the lithology, i.e., it depends on the calcite–quartz–organic matter–phyllosilicate fraction relative amounts. This is the reason why the Aalenian samples from Mizoën ("pelitic layers" on Fig. 7A), which are much richer in phyllosilicates, present different isotopic signatures (i.e., lower $\delta^{18}O$ and $\delta^{13}C$) than all other Liassic marls. These isotopic ratios are in agreement with those analyzed all along the ECM cover, in metapelites (Aalenian samples in Burkhard and Kerrich, 1988; Henry et al., 1996) and metamarls (Burkhard and Kerrich, 1988; Henry et al., 1996; Kirschner et al., 1995) respectively, and reported in Fig. 11. Note that rocks from the La Grave basin (East of our study area) being globally richer in pelitic fraction than our samples, their isotopic signatures are accordingly slightly lower than our Aalenian Mizoën samples (Henry et al., 1996; reported as "ultra-Dauphinois metapelites" in Fig. 11).

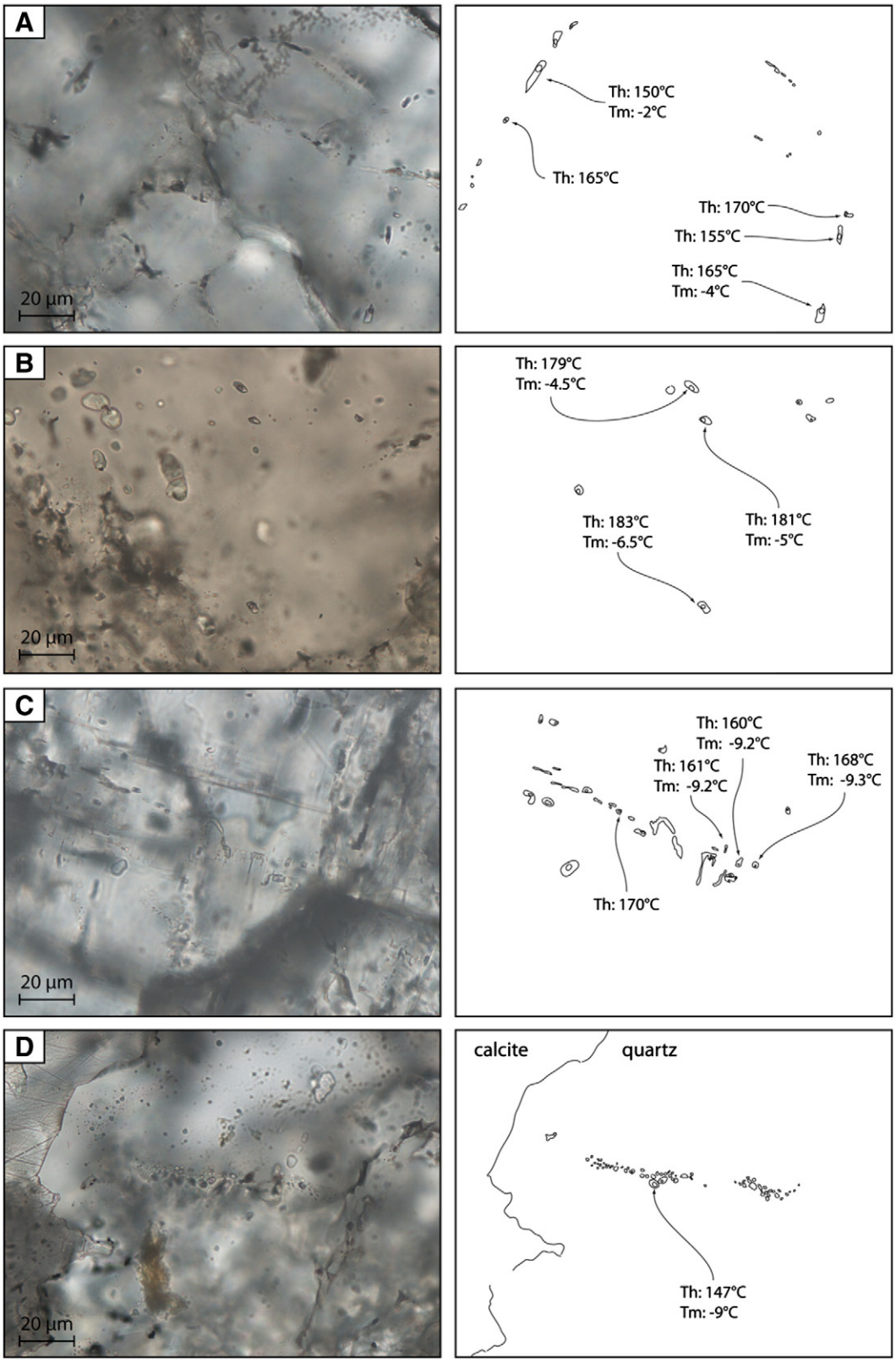

Fig. 8. Microphotographs of thin sections and corresponding sketch of fluid inclusions analyzed by microthermometry. A. Primary fluid inclusions distributed along growth surfaces in a quartz crystal. B. Cluster of primary fluid inclusions in a quartz crystal. C. Pseudo-secondary fluid inclusions in a calcite crystal, aligned along a trail parallel to the vein wall, supposed to develop in response to incremental crystal growth, when the vein-opening rate is lower than the crystal growth rate. D. Trail of pseudo-secondary fluid inclusions in a quartz crystal, parallel to the vein wall.

However, it is noteworthy that although the samples from a specific lithological layer have highly variable calcite–phyllosilicate relative proportions (e.g., Bourg d'Oisans samples in Table 1), their isotopic signatures are very close (Fig. 11), meaning that the rock isotopic composition was equilibrated at the scale of the lithological layer.

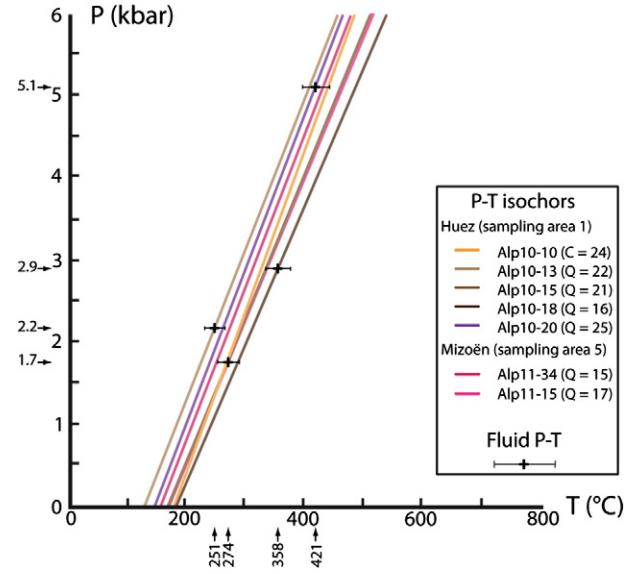

Fig. 9. Isochoric P–T relationships calculated from microthermometric measurements on quartz and calcite crystals from cover veins above the Huez and Mizoën basement shear zones. Host mineral phase and number of measurements are noted for each sample (Q for quartz and C for calcite). The isochors were computed from the homogenization (Th) and melting (Tm) temperatures, using equations from Bodnar (1993) for salinity and from Bodnar and Vityk (1994) for isochor calculations. Fluid temperatures were calculated from $\delta^{18}O$ values of equilibrium quartz and calcite in veins. The error bars are thermometer uncertainties (see Table 2). Fluid pressures are inferred from the intersection of the equilibrium temperatures and the relative isochors.

7.1.2. Fluid flow within the metasedimentary cover: evidence for a nearly-closed fluid system

In both the Bourg d'Oisans and Mizoën basins, calcite isotopic compositions are very similar in veins and associated host-rocks, whatever the vein generation, suggesting local fluid–rock equilibrium in cover rocks all along the successive vein formation. This vein–host-rock isotopic equilibrium precludes massive external fluid influx during deformation (e.g., Burkhard and Kerrich, 1988; Marquer and Burkhard, 1992). Indeed, basement-derived fluids may have very different isotopic signatures, as suggested by the calcite vein analyzed in the Huez basement shear zone (Figs. 7A and 11), and in agreement with the isotopic signature estimated for basement fluids by Henry et al. (1996) (Fig. 11). Therefore, the percolation of important amounts of basement-derived fluids into the overlying cover veins would have modified their isotopic signatures, as observed in the northern ECM basal thrusts of the sedimentary nappes (e.g., Burkhard and Kerrich, 1988; Kirschner et al., 1999) or Glarus thrust (e.g., Burkhard et al., 1992) reported in Fig. 11.

In our rocks, the absence of oxygen isotopic fractionation between host-rock and vein calcite suggests that vein formation occurred at P–T conditions high enough to allow the host-rock mineral isotopic reequilibration mentioned above (i.e., probably close to the peak P–T conditions). Therefore, as indicated by the scale of isotopic reequilibration mentioned above, fluid circulation in the cover rocks was restricted to the scale of the sedimentary formation, i.e., tens to a hundred meter scale. This is supported by observations under cathodoluminescence where calcite from veins and host-rocks exhibits very similar color, whatever the vein generation (Fig. 6G–H), suggesting no evidence of massive external fluid influx in those rocks. Henry et al. (1996) have drawn the same conclusion of a closed-system fluid circulation at the unit-scale for similar cover rocks from the La Grave basin.

Both isotopic and cathodoluminescence homogeneity of calcite in veins and host-rocks thus suggest a local origin for the vein calcite. Dissolution patterns of calcite crystals in the host-rock close to vein walls (Fig. 6A) confirm that calcite was partly dissolved by pressure-solution processes and locally transferred to the successively opening fluid-filled veins where it crystallized. Quartz and calcite pressure-solution and recrystallization in adjacent veins are common deformation mechanisms observed during burial (Bons, 2000; Fisher et al., 1995; Ramsay, 1980; Yardley and Bottrell, 1992) and which have already been described in this area (Gratier and Vialon, 1980; Gratier et al., 1973) and in the northern ECM (Burkhard and Kerrich, 1988; Kirschner et al., 1995). As there is no evidence for infiltration of an important amount of external fluid, diffusive mass transfer likely occurred through the pervasive fluid produced locally by the metamorphic dehydration reactions undergone by clay minerals (i.e., phyllosilicate fraction of the marls) during burial (Cartwright and Buick, 2000; Fisher et al., 1995; Marquer and Burkhard, 1992; Oliver and Bons, 2001; Verlaguet et al., 2011). Making simplified assumptions on the clay mineralogy of the marls protolith (i.e., kaolinite, smectite, illite; see Verlaguet et al., 2011 for further details), modal composition calculations suggest that about 0.1–2 vol.% of fluid may have been produced by metamorphic reactions during the Alpine burial.

However, several authors state that the salinity increase in fluid inclusions from cover veins with the proximity to the Triassic dolomites (Bernard, 1978; Gratier and Vialon, 1980; Gratier et al., 1973; Nziengui, 1993; Poty, 1967) supports the idea of small-scale percolation of Triassic-derived NaCl-rich fluids in the overlying Liassic cover. This is consistent with our salinity data obtained from fluid inclusions in veins from Huez (i.e., just above the Triassic layer, location 1 in Figs. 2, 3A), which correspond to the highest salinity values measured by these authors for the whole Bourg d'Oisans sedimentary cover. Moreover, the isochors calculated from our fluid inclusion microthermometric data (Fig. 9) are in good agreement with those calculated from previous data and reported in Fig. 12 (Bernard, 1978; Gratier et al., 1973; Nziengui, 1993).

On the contrary, the isotopic signature of calcite from Triassic layer veins is clearly different (i.e., lower $\delta^{18}O$ and $\delta^{13}C$) from that of the host-rock calcite (Fig. 7A). This isotopic disequilibrium between Triassic vein and host-rock (Fig. 7B–C) suggests external fluid infiltration through the vein during calcite precipitation. In addition, the Triassic vein isotopic ratio is intermediate between Triassic host-rock and basement isotopic ratios (Figs. 7A, 11), suggesting that the thin Triassic layer underwent basement-derived fluid infiltrations.

7.1.3. Local infiltration of basement-derived fluid in the cover above shear zones

From isotopic data, it can be concluded that there was no massive influx of external fluids in Liassic layers. However, trace element analysis gives complementary insights on the source and scale of fluid circulation. Above the Huez shear zone, veins from Villard-Reculas, situated a few hundred meters above the basement (location 2 in Figs. 2, 3A, 10D), have very similar composition patterns than their host-rocks (Fig. 10C), which is consistent with a local origin of both vein filling elements and fluid (Fig. 10D). On the contrary, in the Huez samples situated just above the sheared basement–cover interface (location 1 in Figs. 2, 3A, 10D), veins present strong relative enrichments in Cr, Co, Ni, Zr, and Hf compared to their host-rock (Fig. 10C). Interestingly, the underlying mafic basement rocks (location 3 in Figs. 2, 3A, 10D) present similar trace element patterns in both sheared and unsheared zones for all elements but Cr, Co, and Ni, suggesting that their concentration may have been modified during shearing: these elements are specifically enriched in the talc-rich zone of the sheared basement (Fig. 10A). Moreover, SEM analysis revealed that, in this talc-rich zone, Ni- and Cr-bearing minerals are Variscan pyrite cores and chromite crystals, respectively (Fig. 5). Both minerals were partially dissolved and replaced by Alpine hydrated phases, as described in detail below, suggesting a release of both Ni and Cr in the infiltrating fluid phase during the Alpine basement shearing.

Therefore, there are clues that small amounts of basement-derived fluids percolated into the cover just above the Huez shear zone (Fig. 10D). However, these fluid amounts must have been very limited: the isotopic signature of this basement-derived fluid, which was

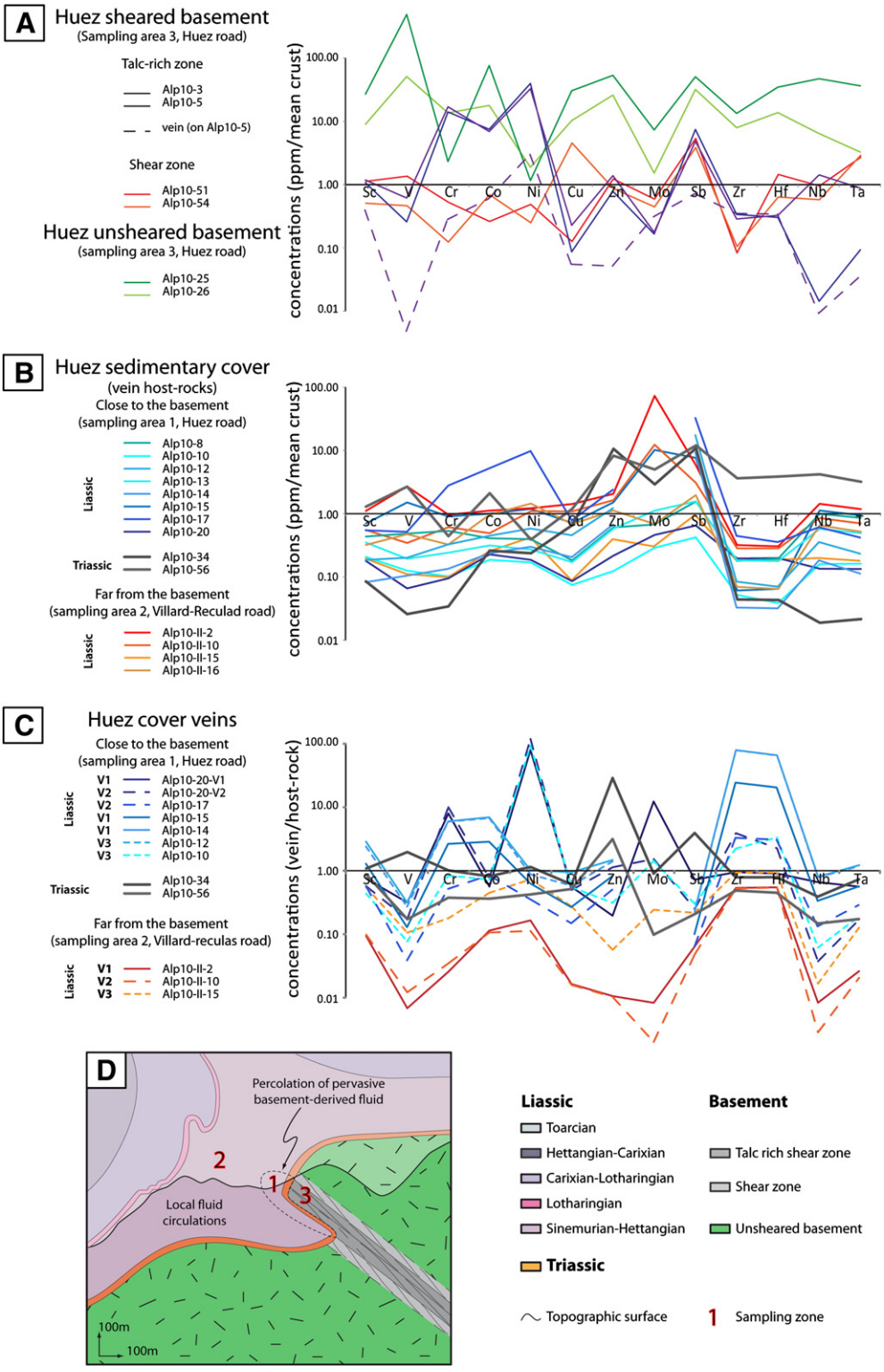

Fig. 10. Trace element patterns for Huez basement shear zone and its sedimentary cover. A. Trace element compositions for Huez basement shear zone and its inner talc-rich zone, and outside the shear zone, normalized to the mean crust (Taylor and McLennan, 1985). B. Trace element compositions for cover host-rocks above the Huez basement shear zone normalized to the mean crust. C. Trace element compositions of cover veins normalized to their host-rock composition, above the Huez basement shear zone. D. Cross-section of the Huez shear zone with sampling area locations, and schematic representation of fluid circulation in the cover above the Huez shear zone. All over the cover, fluid circulations are limited to the sedimentary unit scale, except a few meters above the shear zone, where trace element data provide evidence of spatially-limited basement-derived fluid percolations.

obviously very different from that of cover rocks (i.e., calcite basement vein, Fig. 7A), affected only the Triassic layer (still attached to basement rocks), and was buffered by the isotopic signature of Liassic cover rocks. Moreover, the scale of infiltration of these basement-derived fluids was spatially limited to a few tens of meters in the cover (Fig. 10D). Indeed, in Villard-Reculas (location 2 in Figs. 2, 3A, 10D), the trace element signal of basement-derived fluids is not detected anymore. The very limited flux of percolating fluids through the cover rocks is in agreement with the structural observation that veins are mostly isolated structures and do not constitute a connected network in the metasedimentary

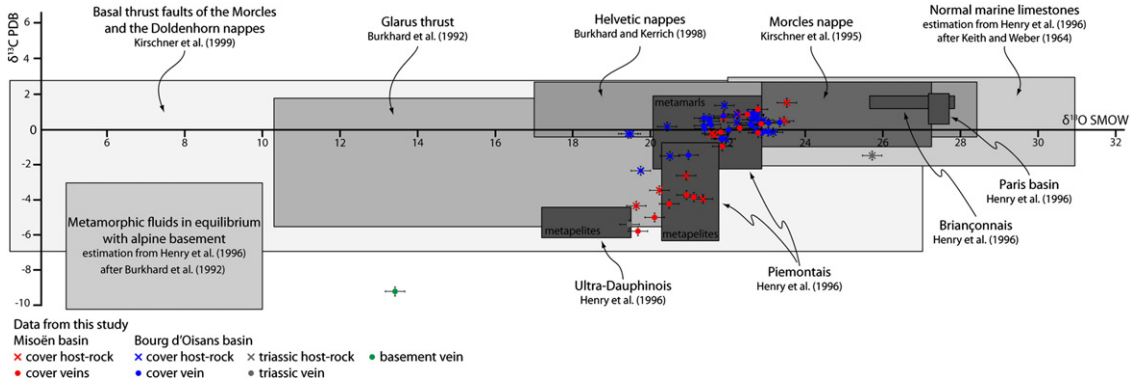

Fig. 11. Isotopic ratios ($\delta^{18}O$ and $\delta^{13}C$) of cover veins and their host-rocks, compared to typical isotopic signatures of different Alpine areas: Ultra-Dauphinois, Briançonnais, Piemontais (Henry et al., 1996), Morcles nappe (Kirschner et al., 1995), all the Helvetic nappes (Burkhard and Kerrich, 1988), and across major tectonic contacts in the ECM cover: the Glarus thrust (Burkhard et al., 1992) and the basal thrust of the Morcles and the Doldenhorn nappes (Kirschner et al., 1999). Typical isotopic signature of marine limestone and calculated isotopic composition of Alpine basement fluids (estimations in Henry et al. (1996), from Burkhard et al. (1992) and Keith and Weber (1964) are also reported.

cover. It is interesting to note that the three successive vein generations of Huez samples present a similar basement-derived trace element signal. Therefore, there is no evidence for significant change in the scale of the fluid system during progressive deformation.

Moreover, in the Triassic dolomites still attached to the sheared basement, sphalerite, pyrite, and galena were observed to have crystallized in calcite fractures. Accordingly, compared to their host-rocks, veins in these Triassic layers show enrichments in some trace elements (Zn ± Sb; Fig. 10B) that are locally concentrated in the underlying talc-rich Huez basement shear zone (Fig. 10A), which supports the hypothesis of local basement-derived fluid percolations into the cover, through the basement–cover interface, above basement shear zones. Interestingly, in La Gardette ancient gold mine (situated in the Bourg d'Oisans basin), similar basement-derived fluid percolation across the unconformity was observed, although this zone is not situated above a basement shear zone: a 500 meter long quartz dyke enriched in sulfur minerals is rooted in the Pelvoux granite (source of the sulfur minerals; Poty, 1967), affects the overlying gneiss and ends in the first 30 m of the Triassic dolomite (Cathelineau et al., 1990; Poty, 1967). However, the source of this local basement fluid circulation remains unclear (Feybesse et al., 2004; Marignac et al., 1997).

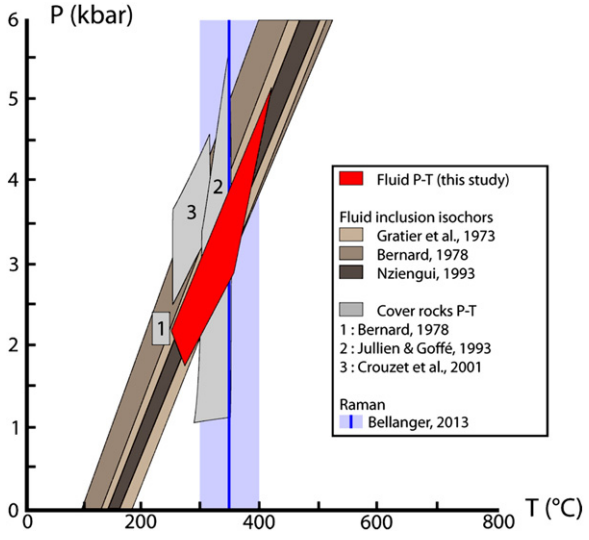

Fig. 12. Fluid P–T range for cover rocks above the Huez shear zone. Fluid temperatures are estimated on the basis of equilibrium temperature between quartz and calcite in veins. Fluid pressures are estimated from fluid temperatures and isochors (PT relationship) computed from microthermometric analysis. Gray zones are P–T conditions determined from (1) fluid inclusion studies in quartz and previous K/Na temperature estimation in albite (Bernard, 1978; Poty et al., 1974); (2) stability of pyrophyllite + margarite + cookeite + quartz + Mg-rich-chlorite (Jullien and Goffé, 1993); (3) previous fluid inclusion studies and Cuire pyrrhotite temperature (Crouzet et al., 2001 and references therein). T max reached by cover rocks (350 °C ± 50 °C) was estimated by RAMAN spectroscopy of the carbonaceous matter (Bellanger, 2013). Brown zones are isochor domains calculated from the microthermometric data (homogenization and melting temperatures) of Bernard (1978), Gratier et al. (1973) and Nziengui (1993), using the equation of Bodnar and Vityk (1994).

Therefore, this study shows that fluid circulations in the Oisans sedimentary cover were restricted to the lithological unit scale, i.e., the fluid system was almost closed. However, when shortening started, small amounts of basement-derived fluids percolated above the basement shear zones into the cover on a few tens of meter scale. These conclusions are in agreement with those of Garofalo (2012) who showed that Alpine marine sediments were generally metamorphosed under closed-system conditions whatever the locality and the metamorphic grade, i.e., element mobility from the sediments is negligible except locally, in narrow shear zones where some specific elements (including Ni and Cr) can be strongly mobilized by the circulation of ascendant fluids.

7.2. Implications for basement fluids

The mobilization of specific elements (Cr, Co, Ni) from basement rocks provides insights into the basement fluid properties during shearing. Samples from the talc-rich area of the Huez basement shear zone (Table 1) show enrichments in Cr, Co, Ni (±Zn and Sb; Fig. 10A) relative to the mean crust, similarly to talc and chlorite schists observed in other settings (e.g., Spandler et al., 2008). The retrogression of the amphibole + plagioclase Variscan paragenesis to Alpine phyllosilicates (chlorite + talc; Fig. 5A) required fluid influx during shearing. Moreover, the partial replacement of the Variscan pyrite crystals by Fe-oxide or hydroxide (i.e., rims around pyrite cores, Fig. 5B) during Alpine fluid infiltration (i.e., linked to talc formation in amphibole cracks) and the partial dissolution of Variscan chromite crystals in Alpine shear zones (Fig. 5C–D–E) suggest a progressive evolution towards more oxidizing conditions in basement rocks with their shearing. Indeed, the internal fluid in equilibrium with the Variscan paragenesis was likely reduced, as shown by the presence of both pyrite and chromite, whereas the external fluid responsible for Alpine phyllosilicate formation had to be more oxidizing.

Interestingly, the pyrite cores are Ni-rich whereas Ni is absent from the Fe-oxide or hydroxide rims, which means that Ni may have been released into the fluid phase during pyrite Alpine oxidation. Similarly, Cr-rich chromite crystals are partially dissolved and surrounded by Cr-rich Alpine chlorite, suggesting Cr release during the Alpine shearing (Fig. 5C–D–E). Therefore, the oxidizing fluid circulating in the basement shear zone may have become enriched in SO_4^{2-} while dissolving sulfur minerals such as pyrite, which was obviously a good complexing anion for metallic elements such as Cr and Ni that were released coevally by

pyrite and chromite partial dissolution. Similar mobilization of metallic low-mobility elements (e.g., Ni, Cr, Zn) by S-rich fluids was observed by Li et al. (2013) and Spandler et al. (2011) in subduction zone settings. This SO_4^{2-} fluid enrichment is supported by the presence of small barytine crystals (identified by SEM) in both the calcite vein in the basement talc-rich zone (Alp10-5, Fig. 10A) and in a Cr–Ni-rich V1 vein in Huez cover rocks, as well as the precipitation of various sulfur minerals (such as sphalerite, galena, pyrite) in Triassic veins above the shear zone. Element mobility was thus clearly controlled by both basement rock mineralogy (enriched in transition metals) and fluid composition, i.e., pH, fO_2 and ligands (e.g., Cathelineau et al., 1990), as was observed for REE complexing and mobility in the Mont Blanc basement shear zones (Rolland et al., 2003).

Small amounts of this basement-derived fluid enriched in transition metals (Cr, Ni) percolated into the overlying metasedimentary cover. Its mixing with the CO_2-rich internally-produced cover fluid, locally at equilibrium with the cover carbonates, may have induced Ni and Cr release in veins within the Lias sediments, and similar sulfur mineral precipitation when percolating through the Triassic layer; the metallic element precipitation may have been caused by sudden changes in fluid pH conditions and X_{CO_2} (e.g., Gao et al., 2007).

7.3. Fluid pressure and temperature in the metasedimentary cover

Here, we combine the analysis of quartz and calcite isotopic signatures in veins to microthermometric measurements of fluid inclusions from the same veins to estimate both the temperature and pressure of the cover vein fluids above basement shear zones. Indeed, quartz and calcite present evidences of textural equilibrium in most veins (Fig. 6F), which implies their co-precipitation under similar P–T conditions. Oxygen isotopic fractionation being essentially dependent on temperature, the temperature of quartz + calcite co-precipitation in veins was estimated from the independent analysis of their $\delta^{18}O$ signature (equation in Sharp and Kirschner, 1994; Table 2).

As most late veins only contain calcite and no quartz, all the veins analyzed in terms of P–T conditions are V1 or early veins (except Alp10-18, Table 2; Fig. 9). Above the Huez shear zone (locations 1 and 2 in Figs. 2–3A), the quartz–calcite equilibrium temperatures range from 144 to 421 °C (±30 °C, Table 2), but most samples plot in the 250–360 °C range (locations 1 and 2 in Table 2). Most of these calculated vein temperatures are consistent with the previous peak temperature estimates for the Bourg d'Oisans and the Mizoën basin cover rocks (300–350 °C, Fig. 12; Bellanger, 2013; Crouzet et al., 2001; Jullien and Goffé, 1993). For a few veins from Huez, combining quartz–calcite equilibrium temperatures to the isochors determined from microthermometric analysis of fluid inclusions in the same quartz or calcite crystals (Fig. 9) provides estimates of the vein fluid pressures (Fig. 12). The fluid pressures range from 1.7 to 5.1 kbar (Fig. 9), which is quite similar to the lithostatic pressure range estimated for the metamorphic peak conditions in these rocks (2–5 kbar, Jullien and Goffé, 1993; Poty et al., 1974; Fig. 12). Gratier and Vialon (1980) estimated fluid pressures of 2 kbar from microthermometric data coupled to temperature data estimated by Poty et al. (1974) for basement vein fluid inclusions (Na/K ratios), which corresponds to the low pressure bound estimated here. However, recalculating the isochors from the microthermometric data of Gratier and Vialon (1980) using the now widely used equation of Bodnar and Vityk (1994) results in steeper isochors (Fig. 12), coherent with ours (Fig. 9), and therefore would undoubtedly tend to higher pressure estimates.

Moreover, as stated before, the $\delta^{18}O$ values for vein calcite are very close to that of the host-rock calcite (Fig. 7A), suggesting that most veins formed close to the peak temperature conditions. However, some V1 veins may have formed during the end of prograde path because (1) the veins are filled by local infiltration of fluid released by prograde metamorphic dehydration reactions into the host-rock and (2) their fluid temperature can be as low as 144 °C.

For the Mizoën basin (locations 4 and 5 in Table 2), the calculated vein temperatures range from 306 to 436 °C, but most temperatures are above 400 °C, which exceeds the estimated peak temperature in the Oisans cover rocks. As discussed in Appendix A.1, these higher values could be the result of an incomplete quartz powder decarbonation for some samples, due to the particularly fine micro-indentation of quartz and calcite in veins.

7.4. Structural implications

In the talc-rich area of basement shear zones, the abundant crystallization of phyllosilicate minerals (talc and chlorite) required the influx of important amounts of external fluids. This talc-rich zone is only a few meters wide inside the shear zone, suggesting that fluid circulation in the basement may have been channelized in the core of the shear zone. Therefore, basement shear zones served as preferential pathways for crustal fluid circulation, as observed in the Mont Blanc (Guermani and Pennacchioni, 1998; Rolland et al., 2003; Rossi et al., 2005) and Aar (Goncalves et al., 2012; Marquer and Burkhard, 1992; Oliot et al., 2010, 2014) basement rocks, as well as in other collisional or subduction-related settings (e.g., Badertscher et al., 2002; Burkhard et al., 1992; John et al., 2008; Kirschner et al., 1999; McCaig et al., 2000a,b). In turn, the crystallization of talc and chlorite may have enhanced deformation localization by progressive softening of these shear zones (Carpenter et al., 2009; Collettini et al., 2009; Moore and Rymer, 2007; Niemeijer et al., 2010) similarly to the weakening effect of the feldspar phengitization (e.g., Bos and Spiers, 2000, 2002; Gueydan et al., 2004; Oliot et al., 2010, 2014).

In northern ECM (e.g., Mont Blanc massif, Rolland et al., 2003), the largest basement shear zones may have propagated as thrusts into the overlying sedimentary cover with ongoing deformation, and became pathways for important amounts of basement-derived fluids, causing meter-scale opening of the fluid system, as recorded by isotopic data in the Aar–Gothard massifs (Burkhard et al., 1992; Kirschner et al., 1999; Marquer and Burkhard, 1992; Fig. 11). In contrast, in the Oisans massif, which underwent less shortening than northern ECM, the basement shear zones did not propagate into the sedimentary cover, preventing important circulation of basement-derived fluids in cover rocks, as shown by isotopic and cathodoluminescence data. Nevertheless, the trace element pattern of cover veins situated just above the basement–cover interface (Huez, location 1 in Figs. 2, 3A) recorded the infiltration of small amounts of basement-derived fluids, whereas in eastern Oisans (La Grave), where the basement is not sheared and the cover decoupled from the basement above a décollement, both isotopic and trace element patterns showed that cover rocks were isolated from basement fluid infiltration (i.e., closed system, Henry et al., 1996).

Even if only small amounts of basement-derived fluids percolated through the interface in western Oisans, they give key insights into the timing of shear zone development and basement shortening. Indeed, the percolation of basement-derived fluids into Huez cover rocks was recorded in the three successive vein generations (V1 to V3), which are all related to the E–W collisional shortening and subsequent basin inversion (Bellahsen et al., 2012; Boutoux et al., 2014; Gratier and Vialon, 1980). Moreover, the basement shear zones are also kinematically consistent with the East–West shortening. Therefore, the percolation of basement-derived fluids into cover veins, which occurred during the entire basin deformation history, unambiguously witnesses that the shortening of the Oisans massif basement began very early during the inversion of the pre-orogenic extensional basins, and lasted during the whole shortening phase. This is supported by geochronology data: the basement shear zone activation was dated to 30–34 Ma in the Pelvoux massif (Simon-Labric et al., 2009), and mineralizations into basement veins give a date of 36–39 Ma (Cathelineau et al., 1990; Marignac et al., 1997; La Gardette gold mine) for basement fluid circulations. The simultaneous deformation of basement and cover basins

during collisional shortening, hence the absence of decoupling between cover and basement, supports an overall thick-skinned structural style.

If most of our cover veins are related to the ductile deformation event (V1, V2 and most V3), it cannot be excluded that part of the V3 veins could be associated to late brittle exhumation phase. Late fluid circulation, from 17 Ma to less than 10 Ma, was evidenced from late vertical veins in basement shear zones from the northern Belledonne and the Aar massifs (Berger et al., 2013; Gasquet et al., 2010), showing that fluid circulation lasted until the brittle exhumation of the ECM.

8. A model for fluid flow in the External Crystalline Massifs

Our results, combined with results of other fluid system studies in the ECM (Abart et al., 2002; Badertscher et al., 2002; Burkhard and Kerrich, 1988; Burkhard et al., 1992; Kirschner et al., 1995, 1999; Marquer and Burkhard, 1992; Rolland et al., 2003) allow proposing a general fluid flow model for the Alpine external zone. This fluid flow model is illustrated together with a schematic kinematic model of the ECM shortening in Fig. 13.

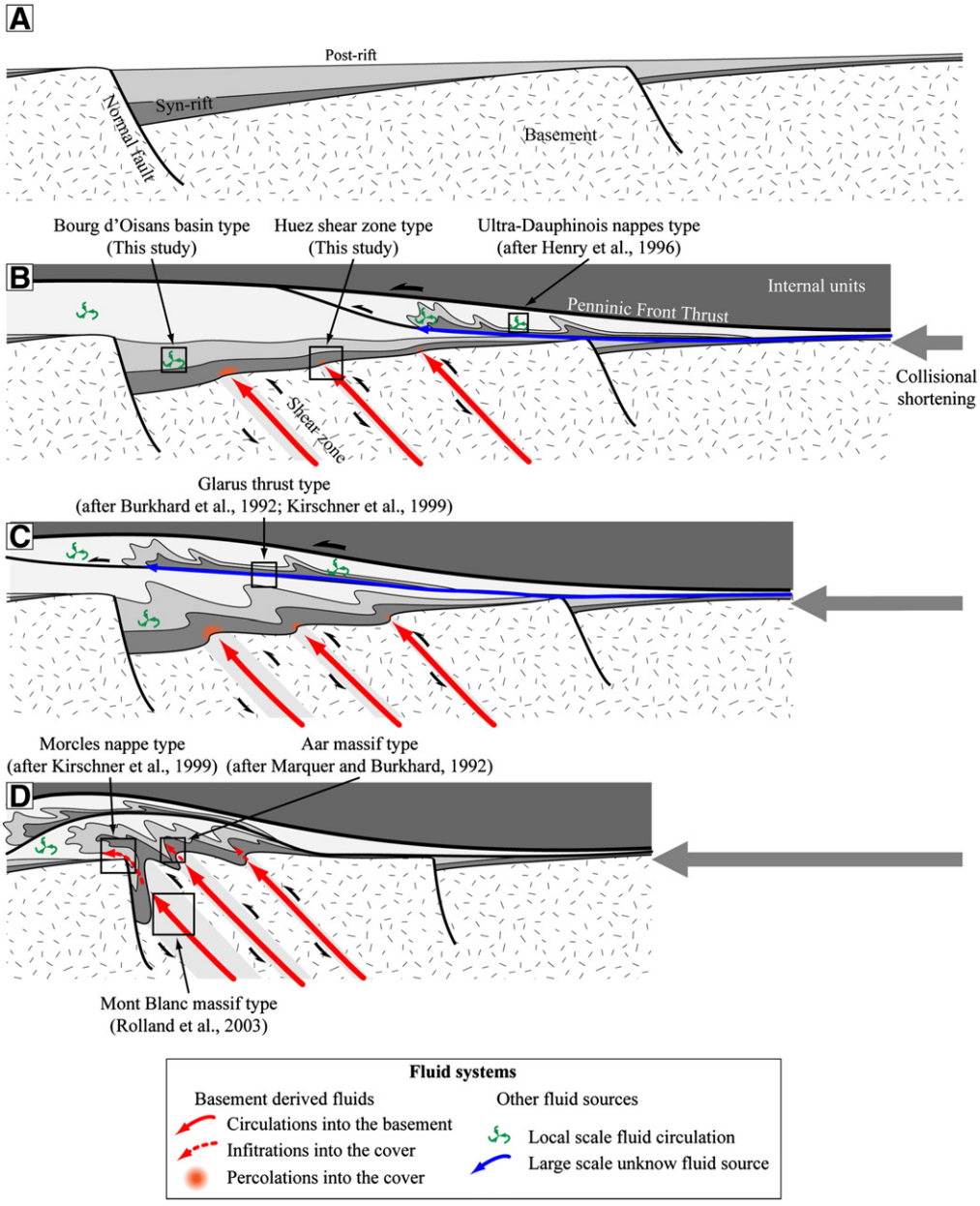

Fig. 13. Fluid system evolution through time and across the strike of the external Alpine Arc, proposed from the compilation of several studies of the fluid system in the ECM and projected on a schematic ECM inherited basin cross-section. A. Initial stage: proximal margin with tilted blocks. B. Initiation of Alpine collisional shortening. The crust is progressively buried to mid-crustal depth under the internal units. In the easternmost part (just below the Penninic Frontal Thrust), the cover is detached from the basement and fluid circulations are restricted to lithologic unit scale above and under the thrusts. In the inherited basins, basement shear zones channelized large-scale fluid circulations, while the cover was disharmonically folded with local-scale fluid circulations and limited basement-derived fluid percolation just above shear zones. C. Higher amount of Alpine collisional shortening. Large sedimentary nappes overthrusted the inverted basins, allowing the channelization of large-scale fluid flow into the thrusts. In inverted basins, fluid channelization into basement shear zones gave rise to important fluid–rock interactions. D. Late Alpine collisional shortening. Fluid circulations in the sedimentary nappes were local at this time and flew across presently inactive thrusts. Inverted basins were progressively pinched and their cover formed recumbent anticlines with overhanging limbs strongly sheared by the basement shear zone propagation, in which basement-derived fluids probably circulated. Within cover nappes, basement-derived fluid flowed up to hundreds of meters above propagated basement shear zones.

The overall tectonic framework is the Alpine burial and collisional shortening of the European crust (see simplified section in Fig. 13A). Probably during the end of the crust burial beneath the internal units, i.e., the end of prograde path (Fig. 13B) or at the metamorphic peak, first ductile deformations initiate (S1 cleavage and associated veins, see Boutoux et al., 2014 for more details). At this stage, for example in the present-day eastern part of the Oisans massif (Ultra-Dauphinois, Fig. 13B), the cover has been locally detached from its basement and progressively overthrusted the western inherited basins. In both the allochthonous and autochthonous units, the fluid system is overall closed (Henry et al., 1996) with isotopic reequilibration restricted to each lithologic unit. However, it is possible that large-scale fluid circulations occurred in the cover thrusts–décollement (thick blue arrow in Fig. 13B), as such zones were not sampled by Henry et al. (1996). Meanwhile, in the western part, the inherited basins (e.g., Oisans massif, Fig. 13B) were progressively shortened and inverted. Shear zones developed within the basement while the overlying cover was disharmonically folded (e.g., Bourg d'Oisans basin, Fig. 13B). Basement-derived fluids were channelized into basement shear zones, and locally infiltrated the overlying cover over a few tens of meters (e.g., the Huez shear zone described in this study, Fig. 13B). In the rest of the cover, i.e., far from basement shear zones, the fluid system remained closed, restricted to the sedimentary unit scale, and involved mainly formational and metamorphic fluids. To sum up, in the Oisans area (Bourg d'Oisans basin, Huez shear zone, Ultra-Dauphinois nappes, Fig. 13B), collisional shortening remained moderate, about 11.5 km (16.1%, Bellahsen et al., 2012, 2014) and thus we face an "immature" fluid system in the cover of the inherited basins.

With increasing shortening, coupled to increasing P–T conditions, basement shear zones developed through the increasing connection of anastomosed shear bands (Marquer and Burkhard, 1992) and were most likely the location of channelized basement-derived fluids (e.g., Aar, Goncalves et al., 2012; Mont Blanc, Rolland et al., 2003) with important fluid–rock interactions, highlighted by REE fractionation (Rolland et al., 2003). In areas where the cover was detached from the basement (e.g., Glarus thrust, Fig. 13C), fluid flow was channelized in the main thrust (Abart et al., 2002; Badertscher et al., 2002; Burkhard and Kerrich, 1988; Burkhard et al., 1992; Kirschner et al., 1999). The related presently one meter-thick calc-mylonite (Schmid et al., 1981) was the locus of δ^{18}O-depleted fluid circulation, as attested by isotopic fronts (e.g., Badertscher et al., 2002), where metamorphic fluids derived from deeper (southern) parts of the thrust mixed with formational fluids northward. The extreme localization of the deformation (1 meter-thick thrust zone) may have permitted a very localized and fast fluid flow that explains the isotopic anomalies. Similar fluid flow probably occurred in the Moine Thrust that is also a very thin and localized thrust accommodating tens of km of shortening (McClay and Coward, 1981). To sum up, in and around the northern ECM (Mont Blanc, Glarus thrust above the Aar massif) where the amount of shortening was higher than in Oisans (10.6 km, 38.3% in the Mont Blanc massif and 12 km, 40% in the Aar massif vs. 11.5 km, 16.1% in the Oisans massif; Bellahsen et al., 2014), the structural style is still a mixed thin- and thick-skinned style. Large-scale fluid flow may occur both in basement shear zones and in large sedimentary nappe thrusts, and may have initiated during the previous step (Fig. 13B) although poorly documented.

In the last step of our model, the structural style switched to a pure thick-skinned style (Fig. 13D), i.e., the shortening was almost exclusively accommodated in basement shear zones. The fluid flow was still active in basement shear zones (Fig. 13D) both in the Mont Blanc (Rolland et al., 2003) and the Aar massifs (Marquer and Burkhard, 1992). The cover of these massifs, the Morcles nappe (Escher et al., 1993) and the Doldenhorn nappe (Burkhard and Kerrich, 1988), respectively, were disharmonically folded as recumbent anticlines with strongly sheared overhanging limbs. Although Burkhard and Kerrich (1988) and Marquer and Burkhard (1992) showed that basement-derived fluids circulated in the major cover thrusts of the Aar massif, the reverse limbs of the above-cited nappes do not systematically bear evidence of large-scale fluid flow (Kirschner et al., 1999; red dashed line in Fig. 13D). These reverse limbs are interpreted as large shear zones (Ramsay et al., 1983). Thus, it appears that the shearing geometry distribution made them less prone to large-scale circulation of important amounts of basement-derived fluids, in contrast to localized structures such as few meter-thick thrust zones, which were efficient drains for localized, large-scale, fluids.

9. Conclusions

In this contribution, we analyzed the fluid system(s) in the inner part of the Alpine External zone, the External Crystalline Massifs (ECM). In this domain, pre-orogenic Liassic extensional basins were buried at mid-crustal depth and inverted during the collisional phase of the Alpine orogeny. During the basin shortening, the sedimentary cover was disharmonically folded over localized basement shear zones. Fluid circulations are associated to this deformation. Isotopic analyses and cathodoluminescence observations show that, as for the ultra-Dauphinois cover nappes, fluid circulations were restricted to local scale in the metasedimentary cover. In the basement shear zones, fluids were channelized as for the other ECM. On the basis of trace element analyses, we highlight the small amount of basement-derived fluid percolation in the metasedimentary cover above such shear zones. Stable ^{18}O isotopic signature coupled to microthermometric analyses of fluid inclusions from cover veins above the Huez basement shear zone provides estimates of fluid temperature and pressure: around 250–400 °C and 2–5 kbar for veins that thus formed close to peak P–T conditions. These veins formed contemporaneously with the onset of and during the basin inversion and basement collisional shortening.

Our study documents the evolution of the fluid system in an area undergoing limited crustal collisional shortening. It therefore nicely complements earlier studies of fluid systems further North in the Western Alps (Mont Blanc and Aar massifs) where the crust suffered more shortening, and allow one to build a consistent conceptual model of fluid flow at the scale of the whole external Alpine collision zone.

Supplementary data to this article can be found online at http://dx.doi.org/10.1016/j.lithos.2014.07.005.

Acknowledgments

The authors thank L. Jolivet and M. Bellanger for discussions and X. and M.O. Gonord for their warm welcome during field trips. Thanks are due to O. Boudouma, M. de Rafelis, N. Labourdette, J. Thibiéroz and E. Delairis for their help with SEM, cathodoluminescence, calcite isotopic analysis, microthermometry and thin section preparation, respectively. Y. Rolland and an anonymous reviewer are acknowledged for their constructive reviews that helped at improving the manuscript. Thanks are due to M. Scambelluri for editorial handling. This study was funded by the "Syster" INSU program, BRGM contract L10 U 044 and ISTeP (UPMC) funds.

References

Abart, R., Badertscher, N., Burkhard, M., Povoden, E., 2002. Oxygen, carbon and strontium isotope systematics in two profiles across the Glarus thrust: implications for fluid flow. Contributions to Mineralogy and Petrology 143 (2), 192–208. http://dx.doi.org/10.1007/s00410-001-0326-5.

Badertscher, N.P., Beaudoin, G., Therrien, R., Burkhard, M., 2002. Glarus overthrust: a major pathway for the escape of fluids out of the Alpine orogen. Geology 30 (10), 875–878. http://dx.doi.org/10.1130/0091-7613(2002)030<0875:GOAMPF>2.0.CO;2.

Barbier, R., Barféty, J.C., Bocquet, A., Bordet, P., Le Fort, P., Meloux, J., Mouterde, R., Pêcher, A., Petiteville, M., 1973. Carte géologique de la France (1/50,000), feuille La Grave (798). Bureau de Recherches géologiques et minières, Orléans.

Barféty, J.C., Bordet, P., Carme, F., Debelmas, J., Meloux, M., Montjuvent, G., Mouterde, R., Sarrot-Reynauld, J., 1972. Carte géologique de la France (1/50,000), feuille Vizille (797). Bureau de Recherches géologiques et minières, Orléans.

Bellahsen, N., Jolivet, L., Lacombe, O., Bellanger, M., Boutoux, A., Garcia, S., Mouthereau, F., LePourhiet, L., Gumiaux, C., 2012. Mechanisms of margin inversion in the external Western Alps: implications for crustal rheology. Tectonophysics 560–561, 62–83. http://dx.doi.org/10.1016/j.tecto.2012.06.022.

Bellahsen, N., Mouthereau, F., Boutoux, A., Bellanger, M., Lacombe, O., Jolivet, L., Rolland, Y., 2014. Collision kinematics in the western external Alps. Tectonics 33. http://dx.doi.org/10.1002/2013TC003453.

Bellanger, M., Bellahsen, N., Jolivet, L., Baudin, T., Augier, R., Boutoux, A., 2014. Basement shear zones development and shortening kinematics in the Ecrins Massif, Western Alps. Tectonics 33 (2), 84–111.

Bellanger, M., 2013. Raccourcissement alpin du massif des Ecrins: Cinématique, calendrier tectonique & conditions pression-température, (Thesis 3e cycle) 2013. Univ Orléans.

Berger, A., Gnos, E., Janots, E., Whitehouse, M., Soom, M., Frei, R., Waight, T.E., 2013. Dating brittle tectonic movements with cleft monazite: fluid–rock interaction and formation of REE-minerals. Tectonics 32 (5), 1176–1189. http://dx.doi.org/10.1002/tect.20071.

Bernard, D., 1978. Microthermométrie des inclusions fluides de cristaux syn-cinématiques. Application à la couverture sédimentaire du Nord Pelvoux. Unpublished PhD Thesis, Univ Grenoble, 133 pp.

Bodnar, R.J., 1993. Revised equation and table for determining the freezing point depression of H_2O–NaCl solutions. Geochimica et Cosmochimica Acta 57 (3) (United States).

Bodnar, R.J., Vityk, M.O., 1994. Interpretation of Microthermometric Data for H_2O–NaCl Fluid Inclusions. Fluid Inclusions in Minerals: Methods and Applications. pp. 117–130.

Bons, P.D., 2000. The formation of veins and their microstructures. Journal of the Virtual Explorer 2, 12.

Bos, B., Spiers, C.J., 2000. Effect of phyllosilicates on fluid-assisted healing of gouge-bearing faults. Earth and Planetary Science Letters 184 (1), 199–210. http://dx.doi.org/10.1016/S0012-821X(00)00304-6.

Bos, B., Spiers, C.J., 2002. Frictional-viscous flow of phyllosilicate-bearing fault rock: microphysical model and implications for crustal strength profiles. Journal of Geophysical Research 107 (B2), 2028. http://dx.doi.org/10.1029/2001JB000301.

Boutoux, A., Bellahsen, N., Lacombe, O., Verlaguet, A., Mouthereau, F., 2014. Inversion of pre-orogenic extensional basins in the external Western Alps: structure, microstructures and restoration. Journal of Structural Geology 60, 13–29. http://dx.doi.org/10.1016/j.jsg.2013.12.014.

Burkhard, M., Kerrich, R., 1988. Fluid regimes in the deformation of the Helvetic nappes, Switzerland, as inferred from stable isotope data. Contributions to Mineralogy and Petrology 99 (4), 416–429. http://dx.doi.org/10.1007/BF00371934.

Burkhard, M., Kerrich, R., Maas, R., Fyfe, W.S., 1992. Stable and Sr-isotope evidence for fluid advection during thrusting of the Glarus nappe (Swiss Alps). Contributions to Mineralogy and Petrology 112 (2-3), 293–311. http://dx.doi.org/10.1007/BF00310462.

Carpenter, B.M., Marone, C., Saffer, D.M., 2009. Frictional behavior of materials in the 3D SAFOD volume. Geophysical Research Letters 36 (5). http://dx.doi.org/10.1029/2008GL036660.

Cartwright, I., Buick, I.S., 2000. Fluid generation, vein formation and the degree of fluid–rock interaction during decompression of high-pressure terranes: the Schistes Lustrés, Alpine Corsica, France. Journal of Metamorphic Geology 18 (6), 607–624. http://dx.doi.org/10.1046/j.1525-1314.2000.00280.x.

Cathelineau, M., Boiron, M.-C., Holliger, P., Poty, B., 1990. Metallogenesis of the French part of the Variscan orogen. Part II: time–space relationships between U, Au and Sn/W ore deposition and geodynamic events — mineralogical and U/Pb data. Tectonophysics 177, 59–79.

Challandes, N., Marquer, D., Villa, I.M., 2008. PTt modelling, fluid circulation, and 39Ar–40Ar and Rb–Sr mica ages in the Aar Massif shear zones (Swiss Alps). Swiss Journal of Geosciences 101 (2), 269–288. http://dx.doi.org/10.1007/s00015-008-1260-6.

Collettini, C., Viti, C., Smith, S.A., Holdsworth, R.E., 2009. Development of interconnected talc networks and weakening of continental low-angle normal faults. Geology 37 (6), 567–570. http://dx.doi.org/10.1130/G25645A.1.

Crouzet, C., Ménard, G., Rochette, P., 2001. Cooling history of the Dauphinoise Zone (Western Alps, France) deduced from the thermopaleomagnetic record: geodynamic implications. Tectonophysics 340 (1), 79–93. http://dx.doi.org/10.1016/S0040-1951(01)00142-1.

Dumont, T., Champagnac, J.D., Crouzet, C., Rochat, P., 2008. Multistage shortening in the Dauphiné zone (French Alps): the record of Alpine collision and implications for pre-Alpine restoration. Swiss Journal of Geosciences 101 (1), 89–110. http://dx.doi.org/10.1007/978-3-7643-9950-4_6.

Dumont, T., Schwartz, S., Guillot, S., Simon-Labric, T., Tricart, P., Jourdan, S., 2012. Structural and sedimentary records of the Oligocene revolution in the Western Alpine arc. Journal of Geodynamics 18–38. http://dx.doi.org/10.1016/j.jog.2011.11.006.

Escher, A., Masson, H., Steck, A., 1993. Nappe geometry in the western Swiss Alps. Journal of Structural Geology 15 (3), 501–509. http://dx.doi.org/10.1016/0191-8141(93)90144-Y.

Etheridge, M.A., 1983. Differential stress magnitudes during regional deformation and metamorphism: upper bound imposed by tensile fracturing. Geology 11 (4), 231–234. http://dx.doi.org/10.1130/0091-7613(1983)11<231:DSMDRD>2.0.CO;2.

Feybesse, J.L., Bailly-Maître, M.C., Feraud, J., 2004. La mine médiévale d'argent du Pontet, une fente alpine contemporaine de la surrection des massifs cristallins? Comptes Rendus Geoscience 336 (14), 1255–1264. http://dx.doi.org/10.1016/j.crte.2004.06.009.

Fisher, D.M., Brantley, S.L., Everett, M., Dzvonik, J., 1995. Cyclic fluid flow through a regionally extensive fracture network within the Kodiak accretionary prism. Journal of Geophysical Research: Solid Earth (1978–2012) 100 (B7), 12881–12894. http://dx.doi.org/10.1029/94JB02816.

Gao, G.Y., Yao, K.L., Şaşıoğlu, E., Sandratskii, L.M., Liu, Z.L., Jiang, J.L., 2007. Half-metallic ferromagnetism in zinc-blende CaC, SrC, and BaC from first principles. Physical Review B 75 (17), 174442. http://dx.doi.org/10.1103/PhysRevB.75.174442.

Garofalo, P.S., 2012. The composition of Alpine marine sediments (Bündnerschiefer Formation, W Alps) and the mobility of their chemical components during orogenic metamorphism. Lithos 128, 55–72. http://dx.doi.org/10.1016/j.lithos.2011.10.009.

Gasquet, D., Bertrand, J.-M., Paquette, J.-L., Lehmann, J., Ratzov, G., Guedes, R.D.A., Tiepolo, M., Boullier, A.-M., Scaillet, S., Nomade, S., 2010. Miocene to Messinian deformation and hydrothermal activity in a pre-Alpine basement massif of the French western Alps: new U–Th–Pb and argon ages from the Lauzière massif. Bulletin de la Société Géologique de France 181, 227–241. http://dx.doi.org/10.2113/gssgfbull.181.3.227.

Goncalves, P., Oliot, E., Marquer, D., Connolly, J.A.D., 2012. Role of chemical processes on shear zone formation: an example from the Grimsel metagranodiorite (Aar massif, Central Alps). Journal of Metamorphic Geology 30 (7), 703–722. http://dx.doi.org/10.1111/j.1525-1314.2012.00991.x.

Gratier, J.P., Vialon, P., 1980. Deformation pattern in a heterogeneous material: folded and cleaved sedimentary cover immediately overlying a crystalline basement (Oisans, French Alps). Tectonophysics 65 (1), 151–179. http://dx.doi.org/10.1016/0040-1951(80)90228-0.

Gratier, J.P., Lejeune, B., Vergne, J.L., 1973. Etude des déformations de la couverture et des bordures sédimentaires des massifs cristallins externes de Belledonne, des Grandes Rousses et du Pelvoux(Thesis 3e cycle) Univ. Grenoble.

Guermani, A., Pennacchioni, G., 1998. Brittle precursors of plastic deformation in a granite: an example from the Mont Blanc massif (Helvetic, western Alps). Journal of Structural Geology 20 (2–3), 135–148. http://dx.doi.org/10.1016/S0191-8141(97)00080-1.

Gueydan, F., Leroy, Y.M., Jolivet, L., 2004. Mechanics of low-angle extensional shear zones at the brittle–ductile transition. Journal of Geophysical Research: Solid Earth (1978–2012) 109 (B12). http://dx.doi.org/10.1029/2003JB002806.

Guillot, S., Ménot, R.P., 2009. Paleozoic evolution of the external crystalline massifs of the Western Alps. Comptes Rendus Geoscience 341 (2), 253–265. http://dx.doi.org/10.1016/j.crte.2008.11.010.

Henry, C., Burkhard, M., Goffe, B., 1996. Evolution of synmetamorphic veins and their wallrocks through a Western Alps transect: no evidence for large-scale fluid flow. Stable isotope, major- and trace-element systematics. Chemical Geology 127 (1), 81–109. http://dx.doi.org/10.1016/0009-2541(95)00106-9.

John, T., Klemd, R., Gao, J., Garbe-Schönberg, C.D., 2008. Trace-element mobilization in slabs due to non steady-state fluid–rock interaction: constraints from an eclogite-facies transport vein in blueschist (Tianshan, China). Lithos 103 (1), 1–24. http://dx.doi.org/10.1016/j.lithos.2007.09.005.

John, T., Gussone, N., Podladchikov, Y.Y., Bebout, G.E., Dohmen, R., Halama, R., Klemd, R., Magna, T., Seitz, H.M., 2012. Volcanic arcs fed by rapid pulsed fluid flow through subducting slabs. Nature Geoscience 5 (7), 489–492. http://dx.doi.org/10.1038/ngeo1482.

Jullien, M.B., Goffé, B., 1993. Occurrences de cookéite et de pyrophyllite dans les schistes du Dauphinois (Isère, France): conséquences sur la répartition du métamorphisme dans les zones externes alpines. Schweizerische Mineralogische und Petrographische Mitteilungen 73, 357–363.

Kirschner, D.L., Sharp, Z.D., Masson, H., 1995. Oxygen isotope thermometry of quartz–calcite veins: unraveling the thermal-tectonic history of the subgreenschist facies Morcles nappe (Swiss Alps). Geological Society of America Bulletin 107 (10), 1145–1156. http://dx.doi.org/10.1130/0016-7606(1995)107<1145:OITOQC>2.3.CO;2.

Kirschner, D.L., Masson, H., Sharp, Z.D., 1999. Fluid migration through thrust faults in the Helvetic nappes (Western Swiss Alps). Contributions to Mineralogy and Petrology 136 (1–2), 169–183. http://dx.doi.org/10.1007/s004100050530.

Keith, M.L., Weber, J.N., 1964. Carbon and oxygen isotopic composition of selected limestones and fossils. Geochim. Cosmochim. Acta 28, 1787–1816. http://dx.doi.org/10.1016/0016-7037(64)90022-5.

Kretz, R., 1983. Symbols for rock-forming minerals. American Mineralogist 68, 277–279.

Leloup, P.H., Arnaud, N., Sobel, E.R., Lacassin, R., 2005. Alpine thermal and structural evolution of the highest external crystalline massif: the Mont Blanc. Tectonics 24 (4), TC 4002. http://dx.doi.org/10.1029/2004TC001676.

Lemoine, M., Gidon, M., Barféty, J.C., 1981. Les massifs cristallins externes des Alpes occidentales: d'anciens blocs basculés nés au Lias lors du rifting téthysien. Comptes Rendus de l'Académie des Sciences Paris 292, 917–920.

Lemoine, M., Dardeau, G., Delpech, P.Y., Dumont, T., De Graciansky, P.C., Graham, R., Jolivet, L., Roberts, D., Tricart, P., 1989. Extension synrift et failles transformantes jurassiques dans les Alpes occidentales. Comptes Rendus de l'Académie des Sciences Série 2 309 (17), 1711–1716.

Li, J.L., Gao, J., John, T., Klemd, R., Su, W., 2013. Fluid-mediated metal transport in subduction zones and its link to arc-related giant ore deposits: constraints from a sulfide-bearing HP vein in lawsonite eclogite (Tianshan, China). Geochimica et Cosmochimica Acta 120, 326–362. http://dx.doi.org/10.1016/j.gca.2013.06.023.

Machel, H.G., Burton, E.A., 1991. Factors governing cathodoluminescence in calcite and dolomite, and their implications for studies of carbonate diagenesis. In: Barker, C.E., Kopp, O.C. (Eds.), Luminescence Microscopy and Spectroscopy: Qualitative and Quantitative Applications. Soc. for Sediment. Geol. , pp. 37–57.

Marignac, C., Cathelineau, M., Bank, D., Boiron, M.-C., Ayt Ougougdal, M., Argouarc'h, Y., Poty, B., 1997. Alpine fault sealing at the contact between a crystalline basement and its sedimentary cover: La Gardette (French Alps). European current research on fluid inclusions. Biennial symposium No 14, Nancy, FRANCE (01/07/1997), pp. 194–195.

Marquer, D., Burkhard, M., 1992. Fluid circulation, progressive deformation and mass-transfer processes in the upper crust: the example of basement–cover relationships in the External Crystalline Massifs, Switzerland. Journal of Structural Geology 14 (8), 1047–1057. http://dx.doi.org/10.1016/0191-8141(92)90035-U.

Marquer, D., Calcagno, P., Barfety, J.C., Baudin, T., 2006. 3D modeling and kinematics of the external zone of the French Western Alps (Belledonne and Grand Châtelard Massifs, Maurienne Valley, Savoie). Eclogae Geologicae Helvetiae 99 (2), 211–222. http://dx.doi.org/10.1007/s00015-006-1183-z.

McCaig, A.M., Wayne, D.M., Marshall, J.D., Banks, D., Henderson, I., 1995. Isotopic and fluid inclusion studies of fluid movement along the Gavarnie Thrust, central Pyrenees; reaction fronts in carbonate mylonites. American Journal of Science 295 (3), 309–343. http://dx.doi.org/10.2475/ajs.295.3.309.

McCaig, A.M., Tritlla, J., Banks, D.A., 2000a. Fluid mixing and recycling during Pyrenean thrusting: evidence from fluid inclusion halogen ratios. Geochimica et Cosmochimica Acta 64 (19), 3395–3412. http://dx.doi.org/10.1016/S0016-7037(00)00437-3.

McCaig, A.M., Wayne, D.M., Rosenbaum, J.M., 2000b. Fluid expulsion and dilatancy pumping during thrusting in the Pyrenees: Pb and Sr isotope evidence. Geological Society of America Bulletin 112 (8), 1199–1208. http://dx.doi.org/10.1130/0016-7606(2000)112<1199:FEADPD>2.0.CO;2.

McClay, K.R., Coward, M.P., 1981. The Moine thrust zone: an overview. Geological Society, London, Special Publications 9 (1), 241–260. http://dx.doi.org/10.1144/GSL.SP.1981.009.01.22.

Moore, D.E., Rymer, M.J., 2007. Talc-bearing serpentinite and the creeping section of the San Andreas fault. Nature 448 (7155), 795–797. http://dx.doi.org/10.1038/nature06064.

Niemeijer, A., Marone, C., Elsworth, D., 2010. Fabric induced weakness of tectonic faults. Geophysical Research Letters 37 (3). http://dx.doi.org/10.1029/2009GL041689.

Nziengui, J.J., 1993. Excès d'argon radiogénique dans les quartz des fissures tectoniques: implications pour la datation des séries métamorphiques(Thesis 3e cycle) L'exemple de la coupe de la Romanche-Alpes occidentales françaisesUniv. Grenoble (209 pp.).

Oliot, E., Goncalves, P., Marquer, D., 2010. Role of plagioclase and reaction softening in a metagranite shear zone at mid-crustal conditions (Gotthard Massif, Swiss Central Alps). Journal of Metamorphic Geology 28 (8), 849–871. http://dx.doi.org/10.1111/j.1525-1314.2010.00897.x.

Oliot, E., Goncalves, P., Schulmann, K., Marquer, D., Lexa, O., 2014. Mid-crustal shear zone formation in granitic rocks: constraints from quantitative textural and crystallographic preferred orientations analyses. Tectonophysics 612–613, 63–80. http://dx.doi.org/10.1016/j.tecto.2013.11.032.

Oliver, N.H., Bons, P.D., 2001. Mechanisms of fluid flow and fluid–rock interaction in fossil metamorphic hydrothermal systems inferred from vein–wallrock patterns, geometry and microstructure. Geofluids 1 (2), 137–162. http://dx.doi.org/10.1046/j.1468-8123.2001.00013.x.

Penniston-Dorland, S.C., Sorensen, S.S., Ash, R.D., Khadke, S.V., 2010. Lithium isotopes as a tracer of fluids in a subduction zone mélange: Franciscan Complex, CA. Earth and Planetary Science Letters 292 (1), 181–190. http://dx.doi.org/10.1016/j.epsl.2010.01.034.

Poty, B., 1967. La croissance des cristaux de quartz dans le filons sur l'exemple du filon de La Gardette (Bourg d'Oisans) et des filons du massif du Mont-Blanc(Thesis 3eme cycle) Univ. Nancy (164 pp.).

Poty, B.P., Stalder, H.A., Weisbrod, A.M., 1974. Fluid inclusions studies in quartz from fissures of Western and Central Alps. Schweizerische Mineralogische und Petrographische Mitteilungen 54 (1974), 717–752.

Ramsay, J.G., 1980. The crack-seal mechanism of rock deformation. Nature 284, 135–139.

Ramsay, J.G., Casey, M., Kligfield, R., 1983. Role of shear in development of the Helvetic fold–thrust belt of Switzerland. Geology 11 (8), 439–442. http://dx.doi.org/10.1130/0091-7613(1983)11<439:ROSIDO>2.0.CO;2.

Roedder, E., 1984. Fluid inclusion, reviews in mineralogy. Mineralogical Society of America 12, 644.

Rolland, Y., Cox, S., Boullier, A.M., Pennacchioni, G., Mancktelow, N., 2003. Rare earth and trace element mobility in mid-crustal shear zones: insights from the Mont Blanc Massif (Western Alps). Earth and Planetary Science Letters 214 (1), 203–219. http://dx.doi.org/10.1016/S0012-821X(03)00372-8.

Rolland, Y., Rossi, M., Cox, S.F., Corsini, M., Mancktelow, N., Pennacchioni, G., Fornari, M., Boullier, A.M., 2008. $^{40}Ar/^{39}Ar$ dating of synkinematic white mica: insights from fluid–rock reaction in low-grade shear zones (Mont Blanc Massif) and constraints on timing of deformation in the NW external Alps. Geological Society, London, Special Publications 299 (1), 293–315. http://dx.doi.org/10.1144/SP299.18.

Rossi, M., Rolland, Y., Vidal, O., Cox, S.F., 2005. Geochemical variations and element transfer during shear-zone development and related épisyénites at middle crust depths: insights from the Mont Blanc granite (French–Italian Alps). In: Bruhn, D., Burlini, L. (Eds.), High Strain Zones: Structure and Physical Properties. Geological Society of London, Special Publications, 245, pp. 373–396.

Salaün, A., Villemant, B., Semet, M.P., Staudacher, T., 2010. Cannibalism of olivine-rich cumulate xenoliths during the 1998 eruption of Piton de la Fournaise (La Réunion hotspot): implications for the generation of magma diversity. Journal of Volcanology and Geothermal Research 198 (1), 187–204. http://dx.doi.org/10.1016/j.jvolgeores.2010.08.022.

Schmid, S.M., Casey, M., Starkey, J., 1981. The microfabric of calcite tectonites from the Helvetic nappes (Swiss Alps). Geological Society, London, Special Publications 9 (1), 151–158. http://dx.doi.org/10.1144/GSL.SP.1981.009.01.13.

Sharp, Z.D., Kirschner, D.L., 1994. Quartz–calcite oxygen isotope thermometry: a calibration based on natural isotopic variations. Geochimica et Cosmochimica Acta 58 (20), 4491–4501. http://dx.doi.org/10.1016/0016-7037(94)90350-6.

Simon-Labric, T., Rolland, Y., Dumont, T., Heymes, T., Authemayou, C., Corsini, M., Fornari, M., 2009. $^{40}Ar/^{39}Ar$ dating of Penninic Front tectonic displacement (W Alps) during the lower oligocene (31–34 Ma). Terra Nova 21 (2), 127–136. http://dx.doi.org/10.1111/j.1365-3121.2009.00865.x.

Spandler, C., Hermann, J., Faure, K., Mavrogenes, J.A., Arculus, R.J., 2008. The importance of talc and chlorite "hybrid" rocks for volatile recycling through subduction zones; evidence from the high-pressure subduction mélange of New Caledonia. Contributions to Mineralogy and Petrology 155 (2), 181–198. http://dx.doi.org/10.1007/s00410-007-0236-2.

Spandler, C., Pettke, T., Rubatto, D., 2011. Internal and external fluid sources for eclogite-facies veins in the Monviso meta-ophiolite, Western Alps: implications for fluid flow in subduction zones. Journal of Petrology 52 (6), 1207–1236. http://dx.doi.org/10.1093/petrology/egr025.

Stünitz, H., 1998. Syndeformational recrystallization—dynamic or compositionally induced? Contributions to Mineralogy and Petrology 131 (2–3), 219–236. http://dx.doi.org/10.1007/s004100050390.

Taylor, S.R., McLennan, S.M., 1985. The Continental Crust: Its Composition and Evolution. Blackwell, Oxford.

Touret, J.L., Frezzotti, M.L., 2003. Fluid inclusion in high pressure and ultrahigh pressure metamorphic rocks. In: Carswell, D.A., Compagnoni, R. (Eds.), Ultrahigh Pressure Metamorphism. Eötvös University Press, Budapest, pp. 467–487.

Tricart, P., Lemoine, M., 1986. From faulted blocks to megamullions and megaboudins: Tethyan heritage in the structure of the Western Alps. Tectonics 5 (1), 95–118. http://dx.doi.org/10.1029/TC005i001p00095.

Verlaguet, A., Goffé, B., Brunet, F., Poinssot, C., Vidal, O., Findling, N., Menut, D., 2011. Metamorphic veining and mass transfer in a chemically closed system: a case study in Alpine metabauxites (western Vanoise). Journal of Metamorphic Geology 29 (3), 275–300. http://dx.doi.org/10.1111/j.1525-1314.2010.00918.x.

Walther, J.V., Orville, P.M., 1982. Volatile production and transport in regional metamorphism. Contributions to Mineralogy and Petrology 79 (3), 252–257. http://dx.doi.org/10.1007/BF00371516.

Wilkin, R.T., Barnes, H.L., Brantley, S.L., 1996. The size distribution of framboidal pyrite in modern sediments: an indicator of redox conditions. Geochimica et Cosmochimica Acta 60 (20), 3897–3912. http://dx.doi.org/10.1016/0016-7037(96)00209-8.

Yardley, B.W.D., Bottrell, S.H., 1992. Silica mobility and fluid movement during metamorphism of the Connemara schists, Ireland. Journal of Metamorphic Geology 10 (3), 453–464. http://dx.doi.org/10.1111/j.1525-1314.1992.tb00096.x.